MECHANISM STUDY OF VIRUS REMOVAL IN MEMBRANE FILTRATION AND THE APPLICATION TO IMPROVE VIRUS REMOVAL

BY

RUIQING LU

DISSERTATION

Submitted in partial fulfillment of the requirements
for the degree of Doctor of Philosophy in Environmental Engineering in Civil Engineering
in the Graduate College of the
University of Illinois at Urbana-Champaign, 2016

Urbana, Illinois

Doctoral Committee:

Associate Professor Thanh H. Nguyen, Chair, Director of Research
Associate Professor Rosa M. Espinosa-Marzal
Assistant Professor Jeremy S. Guest
Associate Professor Moshe Herzberg, Ben Gurion University of the Negev

ABSTRACT

To overcome the severer droughts in recent climate change, direct potable water reuse has been in practice and a wider acceptance can be expected with a reliable control of the water quality. Pathogenic viruses in municipal wastewater can result in outbreaks of virus infection without sufficient removal. Membrane bioreactor (MBR) has shown its promise to remove virus in municipal wastewater treatment, but the major concern is the trade-off between the water permeate flux and the virus removal efficiency. The objective of this study is to understand factors controlling virus removal in low pressure membrane filtration.

The virus transport in the membrane surface vicinity was investigated with the dynamic of virus removal. By filtering human adenovirus 2 (HAdV-2) with a 0.2 μm hollow fiber membrane, the virus removal efficiency was observed to be a function of the number of the total filtered virus (N_v). When N_v was low, the HAdV-2 removal efficiency decreased with N_v, while the permeate flux did not significantly change. The decrease of virus removal was attributed to the accumulation of rejected viruses in the membrane surface vicinity, leading to an increase of the local virus concentration. Further increase of N_v leaded to an increase of virus removal as a function of N_v, accompanied by a decrease of the permeate flux. By fitting the permeate flux decrease with the pore blockage-cake filtration model, it was determined that HAdV-2 fouled the membrane and decreased the effective membrane pore size, leading to the enhanced virus removal and the decreased permeate flux. It was also found that, the aim of high virus removal with the high permeate flux could be achieved by maintaining the pristine membrane and avoiding virus accumulation.

To quantitatively evaluate the virus adsorption on membrane, the adsorption kinetics was investigated with a quartz crystal microbalance with dissipation (QCM-D). Both in the presence and absence of foulants, the HAdV-2 adsorption onto membrane was determined to be irreversible in 3 to 100 mM $CaCl_2$ solutions. The kinetics of HAdV-2 adsorption could be explained with the random sequential adsorption (RSA) model. A decrease of the virus adsorption rate was observed over the adsorption time, because previously adsorbed virions would exert repulsive forces towards the virion approaching the membrane surface. Similar observation was found even in the HAdV-2 favorable adsorption. The knowledge of virus

adsorption indicated that virus adsorbed onto the membrane formed a monolayer to decrease the effective pore size, which enhances the pore blockage and cake layer formation.

The mechanism study illustrates the process of virus passage through the membrane. At the beginning of filtration, the observed high virus removal can be attributed to the virus adsorption onto the pristine membrane surface, and that the local concentration of suspended virus in the membrane surface vicinity is similar to the bulk solution. As filtration goes on, virions adsorbed on the membrane surface repel incoming virions and keep them suspended in the membrane surface vicinity. The convective transport and the diffusive transport jointly push the virus towards the membrane surface, increasing the local virus concentration in the membrane surface vicinity and decreasing the observed virus removal efficiency. In the long-term filtration, the virus adsorption facilitates foulant layer development, which translates into the improved virus removal with the decreased permeate flux.

The mechanism study indicates that to avoid virus adsorption and approaching membrane surface could be effective in maintaining the high virus removal and the high permeate flux at the beginning of filtration. This hypothesis was tested with a zwitterionic polymer grafted membrane. The repulsive interaction forces between incoming particles and the membrane surface was validated with atomic force microscope (AFM) in the contact mode. The repulsive forces keep a distance between viruses and the membrane surface, where the convective force is low since the flow velocity decays with the distance away from the membrane pores. The enhanced virus removal by the grafted membrane was observed in our bench-scale filtration experiment. In the presence of foulants, the permeate flux of the ungrafted membrane significantly decreased while the grafted membrane only had minor decrease in permeate flux. The grafted membrane achieved both higher virus removal and higher membrane permeate flux than the ungrafted membrane in the presence of foulants. The mechanism knowledge is validated by the enhanced virus removal of the grafted membrane. Practically, the zwitterionic polymer grafting method shows its promise to control viruses in water reuse.

ACKNOWLEDGMENTS

I would like to sincerely thank Dr. Thanh H. Nguyen for providing me the chance to pursue a doctoral degree in University of Illinois with her tireless guidance in the last 5 years. Her character of persistent self-improvement encourages me to explore the unknown territories, now and in the future. Her willingness to help and communicate with students is a great source for me to accomplish this dissertation. I also would like to thank Dr. Rosa M. Espinosa-Marzal, Dr. Jeremy S. Guest, and Dr. Moshe Herzberg for their support and serving on my defense committee. Thanks also go to Dr. Benito J. Marinas. His comments in my prelim exam provided great insights and inputs to my work. I would like to thank Dr. David M. Cwiertny, Dr. Volodymyr V. Tarabara, and Dr. Irene Xagoraraki for their research guidance.

My thanks also go to all members in Nguyen group. I appreciate the different scopes brought by the visiting scholars: Qi Li, Jinfeng Lu, Chang Zhang, and Kunquan Li. I learnt a lot of research techniques from my lab mates: Yuanyuan Liu, Nanxi Lv, Shengkun Dong, Yun Shen, Leonardo Gutierrez, Dao Janjaroen, Ofelia C. Remoro, Sahid Rosado, Anthony P. Staub, Annia Vargas, Hanting Wang, Conghui Huang, Miyu Fuzawa, Sital Uprety, Nora Sadik. Thanks to my assistants, Mingming Li and Kazami C. Brockman, for their help in the lab work. I would like to thank Dr. Shaoying Qi for his careful management of the lab and his generous help. It is such a nice experience to study in a harmonious atmosphere.

Finally, I would like to thank National Science Foundation (NSF) for financially supporting the research project.

TABLE OF CONTENTS

CHAPTER 1

INTRODUCTION

1.1 Virus Removal to Ensure Microbial Safety in Water Reuse

With limited water resource and increasing demands for clean water, water scarcity has been a global crisis [1]. In recent years, many regions of the United States are experiencing water shortage because of a series of droughts [2]. Water reuse can be a supplement to water supply: municipal wastewater can be properly treated for multiple water use purposes. Compared to other strategies to increase water supply like sea water desalination, water reuse has the advantage of lower cost [3]. The national public water supply was around 42 billion gallons per day in 2010 [4] and the reused water accounts for less than 1% [3]. The municipal wastewater discharge was estimated to be 32 billion gallons per day nationwide [3]. As the ratio of wastewater being reused is still low, the increase of water reuse can be expected [5].

The lack of public acceptance is a significant obstacle for potable water reuse. Without sufficient treatment, hazardous compounds in reused water can be a threat to public health. The risk of microbial pathogens has always been a concern in water use [6]. Even for non-potable water reuse like irrigation or discharging treated wastewater into the natural environment, the pathogens remained in the water is a threat to human health [7]. In wastewater treatment, pathogen removal is monitored with traditional fecal indicators like fecal coliforms and *Escherichia coli*. These indicators can be used to predict bacteria removal but not for virus removal. Compared to bacteria, viruses are significantly smaller and are different in structure. As a result, the treatment processes in wastewater treatment may achieve much lower virus removal than bacteria [8]. In raw sewage, the concentration of pathogenic viruses is around 10^7 virus/L [9]. After traditional secondary treatment and disinfection, the virus concentration is still around 10^3 virus/L [9]. Considering the low infection dosage of pathogenic viruses [10], current wastewater treatment is far from satisfactory for water reuse.

It was generally accepted that pathogen control should rely on the disinfection process. However, in wastewater treatment, secondary treatment can achieve 2-4 logs virus removal while

disinfection, including ultraviolet or chlorine, can only achieve less than 1 log removal for adenovirus and norovirus [11]. The low removal of viruses by disinfection in wastewater treatment can be due to the organic compounds or ammonia. Because of the negative health effect of disinfection byproducts, to improve the virus removal by increasing disinfectant dosage is not applicable, especially considering the relatively high organic concentration in the treated wastewater [12]. Therefore, it is necessary to remove virus in secondary treatment for water reuse.

1.2 Previous Knowledge on Mechanisms of Virus Removal in Membrane Filtration

High virus removal efficiencies have been shown in membrane bioreactors (MBR) [9, 11, 13, 14]. The high virus removal should be attributed to both the activated sludge and membrane filtration. Microbes in the activated sludge remove viruses through biological inactivation and non-specific virus adsorption. Membrane filtration physically retain viruses but the major contribution of virus removal is from membrane foulants [15-18]. Membrane itself has a relatively low virus removal because membranes used for MBR usually have a nominal pore size larger than viruses. Though foulants increase virus removal, the decrease of water permeability translates into higher energy consumption and more frequent membrane cleaning. Moreover, the low virus removal after membrane cleaning is not acceptable for virus control in water reuse. To remove viruses relying on foulants is not cost-efficient or reliable.

The optimal condition for virus removal by membrane filtration is to achieve higher virus removal without sacrificing the water permeability. To achieve this goal, the mechanism of viruses penetrating the membrane needs to be understood in details. Since the diameter of most viruses is between 20 to 300 nm [19], which is similar to colloids, early research suggested that the virus removal by membrane filtration was achieved through sieving and the efficiency was dominant by the membrane pore size [20]. Recent study showed that, even with the same membrane, the virus removal could be tuned by changing ionic strength and pH of the feed solution [21, 22]. These finding suggests the importance of virus-membrane interaction force in virus transport through membrane. Repulsive interaction forces would inhibit viruses entering

the membrane pores [23], while attractive interaction forces result in virus adsorption onto the membrane [24].

Besides pore size and virus-membrane interaction forces, hydrodynamic forces was also found to influence virus removal [23]. As shown in flow velocity analysis for membrane filtration [25], the water velocity near the membrane pores is much larger than that in the bulk solution. As a result, drag force is pulling viruses towards the membrane pores. Moreover, due to the higher virus concentration in the feed solution than in the permeate solution, virus diffusion also favors virus transport towards the permeate side of the membrane. Since virions moving towards the membrane would get rejected, the local virus concentration in the membrane surface vicinity would be higher than that in the feed solution, which is the concentration polarization of viruses [26]. In summary, membrane pore size, virus-membrane interaction forces, and the hydrodynamic forces jointly determine virus transport through the membrane.

1.3 Objectives

The objective in this study is to determine the mechanisms of virus removal by membrane filtration. Specifically, virus adsorption onto membrane is investigated in the aspects of kinetics, capacity, and reversibility. To simulate the practice in water reuse, virus adsorption was studied both in the presence and absence of foulants. A wide range of ionic conditions including that of the municipal wastewater is tested to determine the dominant factor in virus adsorption. The influence of virus behaviors, including adsorption and accumulation on the membrane surface, on the observed virus removal efficiency is determined in lab-scale filtration units. The dynamic of virus removal is studied with different virus concentration in the feed solution. By monitoring the virus removal and the membrane permeate flux, the relationship between virus transport and virus removal can be determined. The role of repulsive forces inhibiting virus approaching the membrane surface is highlighted in the mechanism study.

The role of repulsive virus-membrane interaction forces in virus removal is examined in the second part to test our hypothesis in the mechanism study. The membrane surface with repulsive surface forces can be acquired with a zwitterionic polymers grafted membrane. The virus removal is investigated in filtration units so as to determine how is the virus removal changed by

the repulsive interaction forces. The filtration experiment results are compared with our hypothesis in the mechanism study to reveal the significance of surface repulsive forces in virus removal.

1.4 Experiment Design

Two viruses, bacteriophage MS2 and human adenovirus type 2 (HAdV-2) were used as model viruses in this study. MS2 is a surrogate for the pathogenic human norovirus for their similarity in size and structure [27]. MS2 has also been widely used as virus indicators in water and wastewater treatment. HAdV-2 is a representative for all types of pathogenic human adenoviruses causing respiratory and diarrhea diseases [28]. The size of MS2 (around 30 nm in diameter) and HAdV-2 (around 170 nm in diameter) cover the range of most viruses. Propagation, purification, quantification, and characterization of viruses were conducted before the filtration experiments.

Soluble microbial products (SMP) and extracellular polymeric substances (EPS) were extracted from activated sludge and used as model foulants in the filtration and adsorption experiments [29]. The activated sludge was sampled from a full scale MBR in Traverse City, Michigan. Concentrations of SMP and EPS were determined in total organic carbon (TOC) with a Shimadzu TOC analyzer. The ionic condition of the activated sludge was studied with an inductively coupled plasma mass spectrometry (ICP-MS). Based on the ICP-MS results, 3 mM $CaCl_2$ at pH=8.0 buffered with $NaHCO_3$ was set as the ionic condition throughout the study.

Bench-scale membrane filtration units were set up for both hollow fiber membrane and flat sheet membrane. The filtration units were operated in either the constant flow rate or the constant pressure mode. The operation mode was controlled with a peristaltic pump (Model 7523–70, Masterflex). A pressure gauge and an electronic balance were connected to a computer to record the pressure and permeate flow rate in real-time. The observed virus removal efficiency was determined with the virus concentrations in the feed and the permeate solutions.

The virus adsorption onto membrane was studied in a quartz crystal microbalance with dissipation (QCM-D 300). The QCM-D sensors were supplied by Biolin Scientic (Sweden) and the gold sensor surface was coated with polymers that are used for membrane production.

Solutions were introduced into the QCM-D chamber with a Harvard syringe pump. The flow rate was fixed to 0.1 mL/min to maintain the Reynold number at 1.0. The changes of both frequency and dissipation shift during adsorption were recorded. The kinetics of virus adsorption could be appropriately explained with the random sequential adsorption model.

Interaction forces between viruses and membranes were investigated with an Asylum atomic force microscope (AFM) in the contact mode. Fresh sliced mica surface was used a control surface before and after force measurement to ensure the reliability of the probes. Besides force measurement, AFM was also used in the tapping mode to determine the topography of the membrane surface.

1.5 Dissertation Organization

Chapter 2 is titled as "Effect of virus influent concentration on its removal by microfiltration: The case of human adenovirus 2". The virus removal was determined to be influenced by virus adsorption and accumulation on membrane surface. With the increase of the total number of filtered viruses, the virus removal decreased at the beginning and then increased. During the decrease of the virus removal, the permeate flux was observed to be unchanged, while the increase of virus removal was accompanied by a decrease of the permeate flux. The decrease of virus removal at the beginning of the filtration was attributed to virus accumulation on the membrane surface, leading to an increase of the local virus concentration in the membrane surface vicinity. As the filtration went on, the local virus concentration increased to a limit, and virions fouling the membrane resulted in the increase of virus removal. The permeate flux was fitted with the pore blockage and cake filtration model to confirm virus fouling membrane. Both pore restriction and pore blockage were detected for virus fouling the membrane. Results in this chapter indicates the significance of virus-membrane interaction forces and hydrodynamic forces on virus removal.

Virus adsorption onto membranes was quantitatively investigated in Chapter 3 with the title "Random sequential adsorption of human adenovirus 2 onto polyvinylidene fluoride surface influenced by extracellular polymeric substances". HAdV-2 adsorption was studied in 3-100 mM $CaCl_2$ solutions in QCM-D both in the presence and absence of EPS as membrane foulants. The

HAdV-2 adsorption was found to be irreversible in all conditions. The adsorption rate was found to decay with the adsorption time, indicating that monolayer adsorption might occur. The adsorption kinetics was found to be appropriately explained with the random sequential adsorption model. The area occupied by each virus was found to be influenced by the $CaCl_2$ concentration and the EPS foulants because of the change of the virus-virus and virus-membrane forces. The importance of virus-membrane interaction forces was confirmed in the favorable adsorption of HAdV-2. The strong electrostatic attractive force between HAdV-2 and the positively charged surface surpass the repulsive virus-virus interaction forces. Therefore, the fibers of HAdV-2 overlapped and the area occupied by each adsorbed virus is close to the icosahedral nucleocapsid of HAdV-2. Findings in this chapter suggest that tuning the virus-membrane interaction forces would be effective in changing virus adsorption onto membrane.

The title of Chapter 4 is "Modifying ultrafiltration membranes with zwitterionic grafted polymers for improved virus removal". Based on the mechanism knowledge gained in Chapter 2 and 3, repulsive virus-membrane interaction force was introduced to improve the virus removal efficiency. The redox initiated polymerization was conducted under pressure to graft zwitterionic polymers onto the membrane surface and within the membrane pores. The AFM force measurement detected stronger repulsive force on the modified membrane than the unmodified membrane. The modified membrane achieved 4 logs higher virus removal for both MS2 and HAdV-2, while the permeate flux was around 20% lower than the unmodified membrane. After fouled by SMP, the modified membrane had a higher virus removal and a higher permeate flux for both MS2 and HAdV-2. The mechanism knowledge in Chapter 2 and 3 is proved in this chapter. The zwitterionic graft polymerization showed its promise to control virus in water reuse for the enhanced virus removal.

All findings above are summarized in Chapter 5 to show the contribution and implication of this work. The studies in Chapter 2 and 3 have been published in peer review journals. Chapter 4 is in preparation for submission to Water Research. The published papers are listed below:

1. Lu, R., et al., *Effect of virus influent concentration on its removal by microfiltration: The case of human adenovirus 2*. Journal of Membrane Science, 2016. **497**: p. 120-127.

2. Lu, R., Q. Li, and T.H. Nguyen, *Random sequential adsorption of human adenovirus 2 onto polyvinylidene fluoride surface influenced by extracellular polymeric substances*. Journal of Colloid and Interface Science, 2016. **466**: p. 120-127.

1.6 References

1. Watkins, K., *Human Development Report 2006-Beyond scarcity: Power, poverty and the global water crisis.* UNDP Human Development Reports (2006), 2006.
2. Devineni, N., et al., *America's water risk: Current demand and climate variability.* Geophysical Research Letters, 2015. **42**(7): p. 2285-2293.
3. Reuse, W., *Potential for Expanding the Nation's Water Supply through Reuse of Municipal Wastewater (2012).* Water reuse: potential for expanding the nation's water supply through reuse of municipal wastewater, National Research Council, 2012.
4. Maupin, M.A., et al., *Estimated use of water in the United States in 2010*. 2014, US Geological Survey.
5. Wade Miller, G., *Integrated concepts in water reuse: managing global water needs.* Desalination, 2006. **187**(1–3): p. 65-75.
6. Cisneros, B.E.J., B. Jimenez, and T. Asano, *Water reuse: an international survey of current practice, issues and needs*. 2008: IWA Publishing.
7. Wong, M., et al., *Evaluation of public health risks at recreational beaches in Lake Michigan via detection of enteric viruses and a human-specific bacteriological marker.* Water Research, 2009. **43**(4): p. 1137-1149.
8. USEPA, *Guidelines for Water Reuse, Office of Wastewater Management, Washington, DC. EPA/600/R-12/618.* 2012.
9. Simmons, F.J., D.H.W. Kuo, and I. Xagoraraki, *Removal of human enteric viruses by a full-scale membrane bioreactor during municipal wastewater processing.* Water Research, 2011. **45**(9): p. 2739-2750.
10. Xagoraraki, I., Z. Yin, and Z. Svambayev, *Fate of Viruses in Water Systems.* Journal of Environmental Engineering, 2014. **140**(7).
11. Simmons, F.J. and I. Xagoraraki, *Release of infectious human enteric viruses by full-scale wastewater utilities.* Water Research, 2011. **45**(12): p. 3590-3598.

12. Krasner, S.W., et al., *Occurrence of Disinfection Byproducts in United States Wastewater Treatment Plant Effluents.* Environmental Science & Technology, 2009. **43**(21): p. 8320-8325.
13. Madaeni, S.S., *The application of membrane technology for water disinfection.* Water Research, 1999. **33**(2): p. 301-308.
14. Zheng, X., et al., *Evaluation of virus removal in MBR using coliphages T4.* Chinese Science Bulletin, 2005. **50**(9): p. 862-867.
15. Lv, W., et al., *Virus removal performance and mechanism of a submerged membrane bioreactor.* Process Biochemistry, 2006. **41**(2): p. 299-304.
16. Shang, C., H.M. Wong, and G.H. Chen, *Bacteriophage MS-2 removal by submerged membrane bioreactor.* Water Research, 2005. **39**(17): p. 4211-4219.
17. Wu, J., H. Li, and X. Huang, *Indigenous somatic coliphage removal from a real municipal wastewater by a submerged membrane bioreactor.* Water Research, 2010. **44**(6): p. 1853-1862.
18. Lu, R., D. Mosiman, and T.H. Nguyen, *Mechanisms of MS2 Bacteriophage Removal by Fouled Ultrafiltration Membrane Subjected to Different Cleaning Methods.* Environmental Science & Technology, 2013. **47**(23): p. 13422-13429.
19. Lamb, R.A., R. Krug, and D. Knipe, *Fields virology.* Fields Virology, 2001. **1**.
20. Mallevialle, J., P.E. Odendaal, and M.R. Wiesner, *Water treatment membrane processes*. 1996: American Water Works Association.
21. Dishari, S.K., et al., *Effects of solution conditions on virus retention by the Viresolve® NFP filter.* Biotechnology Progress, 2015. **31**(5): p. 1280-1286.
22. Skibinski, B., P. Müller, and W. Uhl, *Rejection of submicron sized particles from swimming pool water by a monolithic SiC microfiltration membrane: Relevance of steric and electrostatic interactions.* Journal of Membrane Science, 2016. **499**: p. 92-104.
23. Kim, M.-m. and A.L. Zydney, *Effect of electrostatic, hydrodynamic, and Brownian forces on particle trajectories and sieving in normal flow filtration.* Journal of Colloid and Interface Science, 2004. **269**(2): p. 425-431.
24. Lukasik, J., et al., *Influence of salts on virus adsorption to microporous filters.* Applied and Environmental Microbiology, 2000. **66**(7): p. 2914-2920.

25. Pontius, F.W., J.P. Crimaldi, and G.L. Amy, *Virus passage through compromised low-pressure membranes: A particle tracking model.* Journal of Membrane Science, 2011. **379**(1–2): p. 249-259.
26. Jackson, N.B., et al., *Internal virus polarization model for virus retention by the Ultipor® VF Grade DV20 membrane.* Biotechnology Progress, 2014. **30**(4): p. 856-863.
27. Bae, J. and K.J. Schwab, *Evaluation of murine norovirus, feline calicivirus, poliovirus, and MS2 as surrogates for human norovirus in a model of viral persistence in surface water and groundwater.* Applied and Environmental Microbiology, 2008. **74**(2): p. 477-484.
28. Jiang, S.C., *Human Adenoviruses in Water: Occurrence and Health Implications: A Critical Review†.* Environmental Science & Technology, 2006. **40**(23): p. 7132-7140.
29. Liu, H. and H.H.P. Fang, *Extraction of extracellular polymeric substances (EPS) of sludges.* Journal of Biotechnology, 2002. **95**(3): p. 249-256.

CHAPTER 2

EFFECT OF VIRUS INFLUENT CONCENTRATION ON ITS REMOVAL BY MICROFILTRATION: THE CASE OF HUMAN ADENOVIRUS 2

Published in *Journal of Membrane Science*, 2016

Lu, R., et al., *Effect of virus influent concentration on its removal by microfiltration: The case of human adenovirus 2*. Journal of Membrane Science, 2016. **497**: p. 120-127.

2.1 Abstract

For safe water reuse, pathogenic viruses need to be efficiently controlled. Membrane filtration is considered to be an effective technology for virus removal. The present work explores mechanisms of human adenovirus 2 (HAdV-2) removal by a hollow fiber microfiltration membrane (d_{pore}= 0.2 μm) as a function of influent virus concentration ranging from 1.3×10^7 to 3.4×10^8 copies/mL. A gradual decrease of HAdV-2 removal over time was observed at the beginning of filtration and was attributed to the accumulation of rejected HAdV-2 at the membrane surface or within membrane pores. Flux decline analysis revealed that complete pore blocking and standard pore blocking dominated the early stages of filtration and then transitioned to cake filtration at longer filtration times as the primary reason for flux decline. Deposition of HAdV-2 onto the membrane during the later stages of filtration led to the formation of a partly irreversible fouling layer and an increase of HAdV-2 removal. The understanding of HAdV-2 behavior at the membrane surface revealed in this study can help with the development of antifouling membranes with high virus removal efficiency.

2.2 Introduction

With population and water demand growing, ever increasing water scarcity has driven water reuse in the United States and other countries [1]. Municipal wastewater is currently regarded as an important resource rather than waste. Treatment technologies have enabled non-potable reuse of treated municipal wastewater for irrigation, aquifer recharge, and application in various

industries [2]. The potable reuse, however, is still very limited in practice [3]. For both potable and non-potable reuse of municipal wastewater, a sufficient removal of pathogens, including the smallest microorganisms – viruses - is required to ensure public safety. For example, human adenovirus (HAdV), one of the most commonly found waterborne viral pathogens [4-6], was found at concentrations higher than 10^3 virus/L by qPCR even after disinfection at five wastewater treatment plants in Michigan [7]. These results suggest the need for novel advanced technology instead of conventional treatment to ensure virus removal in wastewater treatment facilities. Full scale membrane bioreactors (MBRs) were proven to achieve better virus removal compared to conventional wastewater treatment, which rely on the activated sludge process as the secondary treatment [7]. However, the major challenge with membrane filtration, especially for wastewater treatment, is the cost associated with controlling membrane fouling [8-10]. For this reason, significant efforts have been put forth to understand fouling mechanisms [11-13] and to develop fouling-resistant membranes and operational strategies that minimize permeate flux decline caused by membrane fouling [14-19].

The efficiency of virus removal by membranes of different pore size has been examined using bacteriophages as surrogates for pathogenic viruses. Microfiltration membranes achieve 1 - 2 logs (90 to 99%) virus removal while affording much higher permeate flux than ultra- or nanofiltration membranes [20, 21]. New microfiltration membrane designs have been explored to achieve high virus removal without losing the benefit of the high permeate flux, and efforts have been made to incorporate virus removal as a criterion in developing new membranes [22]. However, the lack of detailed understanding of virus removal mechanisms prevents these efforts from translating into practical benefits. Membrane separation and fouling are essentially the consequences of surface interactions. Therefore, knowledge on virus behavior in the vicinity of the membrane surface is important for achieving an optimal combination of virus removal and high permeate flux. HAdV-2 are biological colloids that consist of a protein capsid and a double stranded DNA in the virus core [23]. Previous findings on either model colloids [24, 25] or model proteins [26, 27] can be helpful but inadequate in understanding the behavior of HAdV-2 in the membrane vicinity.

To fill the knowledge gap mentioned above we studied the effects of virus concentration near the membrane surfaces on virus removal. A bench-scale microfiltration unit was employed to

investigate the dynamics of virus removal and membrane permeate flux as a function of influent concentration of the virus. We used human adenovirus type 2 (HAdV-2), as a model pathogenic virus, because HAdV-2 is frequently detected in municipal wastewater [4, 28, 29]. We hypothesize that during the initial stage of filtration, HAdV-2 removal efficiency is influenced by the influent concentration of the virus, as found for other model colloids [30]. This hypothesis was tested by monitoring permeate flux and HAdV-2 removal over the filtration time for different influents concentrations of HAdV-2. If the flux decline is hydraulically reversible (i.e., the permeate flux can be recovered to that of the clean membrane when the transmembrane pressure differential decreased to zero), we expect that HAdV removal would also be recovered [24]. If the flux decline is hydraulically irreversible, and a gel or cake layer is formed on the membrane surface [25], we expect that HAdV removal would be affected by the fouling layer. We applied a combined pore blockage-cake filtration model (PB-CF) [26] to elucidate virus behavior in the immediate vicinity of membrane pore surfaces. By correlating the observed virus removal and fouling mechanisms revealed by the PB-CF model, we draw conclusions on how and why virus removal depends on the influent virus concentration and the filtration time. Future efforts will focus on HAdV removal in the presence of other foulants and by membranes with antifouling surfaces.

2.3 Methods

HAdV-2 propagation and purification. HAdV-2 (ATCC, VR-846) was propagated in the A549 human lung carcinoma cells (Diagnostic Hybrids). Before inoculation with HAdV-2, the A549 cells were propagated in cell culture flasks at 37 ^{0}C in a 5% CO_2 incubator. The growth medium used for A549 cell propagation was Ham's F12K growth media supplemented with 10% fetal bovine serum (FBS), 100 U/ml of penicillin, 100 µg/ml of streptomycin, and 0.25 µg/ml of amphotericin B [31]. Once the A549 cells in the flask reached 80-90% confluence, they were inoculated with HAdV-2. The growth media used for HAdV-2 amplification was similar to the one used for A549 propagation except that 2% FBS was supplemented. The cytopathic effect of the A549 cells was observed 3 to 4 days after inoculation. HAdV-2 was released from the A549 cells by 3 cycles of freezing in -80 ℃ and thawing in 4 ℃. The suspension after lysis was

centrifuged at 230g for 10 min to precipitate cell debris. The supernatant was filtered with a 0.45 μm pore size cellulose acetate membrane (Corning CLS431155) to further remove cell debris. The filtrate was concentrated and further purified using a 100 kDa ultrafiltration membrane (Koch HFM-180) housed in an Amicon stirred cell (Millipore) to remove residues of the growth media. By repeatedly adding sterile 1 mM $NaHCO_3$ solution into the stirred cell, the media residue in the HAdV-2 suspension was washed away. The concentration of HAdV-2 in the resulting stock suspension was measured with quantitative real-time PCR (qPCR) as described below.

HAdV-2 hydrodynamic diameter measurements. The measurements of HAdV-2 hydrodynamic diameter were performed using a method similar to a procedure described previously [32, 33]. Briefly, dynamic light scattering (DLS) tests were conducted using Zetasizer (ZS90, Malvern). The concentration of HAdV-2 in the measurement was diluted to 3×10^8 virus/mL in 3 mM $CaCl_2$ solution at pH=8.0 buffered by $NaHCO_3$. The ionic composition and pH were chosen to match those in our previous measurement of municipal wastewater from a full-scale wastewater treatment plant in Traverse City, Michigan [32]. The measurements were performed immediately after the sample preparation and 1 day afterwards to study whether HAdV-2 had aggregated. Each measurement included 3 replicates.

Quantification of HAdV-2 by qPCR. qPCR was applied to quantify HAdV-2 concentration with a protocol modified from the one reported previously [34]. The genome of HAdV-2 was extracted with PureLink Viral RNA/DNA Mini Kit (Invitrogen, USA). The conserved Hexon gene in the HAdV-2 genome (nt. 18856 – 19137 in HAdV-2 sequence) was the qPCR amplification region. Primers for the amplification region are as follows: AQ1 (5'-GCC-ACG-GTG-GGG-TTT-CTA-AAC-TT-3') and AQ2 (5'-GCC-CCA-GTG-GTC-TTA-CAT-GCA-CAT-C-3'). Templates of qPCR standard curves were acquired with the double stranded DNA of the Hexon gene. This DNA standard was produced by Integrated DNA Technologies (Coralville, IA). A blank sample with molecule biology grade water (Corning) was always run with standard curves and unknown samples. The reaction mix of qPCR included 7.5 μL Power SYBR Green PCR Master Mix (Life Technology, NY), 2 μL templates (standards, samples or blank), 1.5 μL of each primer to get a final concentration of 0.5 μM, and 2.5 μL of PCR-grade water. Reaction was performed in a BioRad MiniOptical Real-Time PCR system. The reaction started with 95 ℃

for 10 min to activate DNA polymerase, followed by 45 cycles of denaturation at 95 ℃ for 3 s, annealing at 55 ℃ for 10 s and extension at 60 ℃ for 1 min with fluorescence signal measured at the end of each cycle. The threshold of fluorescence signal and cycle numbers to achieve the threshold for each sample are calculated automatically by Sequence Detection Systems Software 2.4 (Applied Biosystems, CA). For the standard curves, qPCR reaction was run with serial dilution of the Hexon gene DNA standard as templates at concentration from 1.3×10^2 to 1.3×10^6 genome equivalent (copies)/run. The reaction of 1.3×10^1 copies/run was only occasionally detected, while concentrations higher than or equal to 1.3×10^2 copies/run were constantly detected. Blank samples were not detected in all reactions. A standard curve was generated with freshly prepared serial dilution of the Hexon gene DNA standard for every set of qPCR. Using the cycle numbers achieving the threshold as the y axis and the $\log_{10}$ value of gene copy numbers as the x axis, the average slope was -3.43±0.12 for 10 standard curves in total, and the coefficients of determination (R^2) were all higher than 0.99. The average amplification efficiency was 95% calculated from the average slope of the standard curves.

HAdV-2 removal by a hollow fiber microfiltration membrane. The HAdV-2 removal and the permeate flux were monitored in filtration experiments that used a hollow fiber filtration unit operated in the constant pressure mode (Figure 2.1), as described in previous studies [32, 35]. The pressure controller installed in the retentate line downstream of the membrane kept the transmembrane pressure at 0.4 bar throughout the filtration process. The influent was pumped into the filtration unit by a peristaltic pump (Model 7523-70, Masterflex). A pressure indicator was installed to monitor the transmembrane pressure, allowing manual adjustment of the influent flow rate to match the permeate flow rate. The retentate flux was only ~ 0.05×10^{-5} m/s, which was more than an order of magnitude smaller than the permeate flux that ranged between 5.0×10^{-5} m/s at the beginning of filtration and 0.7×10^{-5} m/s at the end of filtration. Thus, the experimental conditions closely approximated the dead-end filtration mode.

The filtration tests were performed using a hollow fiber polyethersulfone membrane with a nominal pore size of 0.2 μm (M2-M02E-600-F1N, SpectrumLabs). The permeate flux of the membrane was measured by collecting filtrate on an electronic mass balance. The balance and pressure gauge readings were automatically recorded by a computer at 5 s intervals. 3 mM $CaCl_2$ at pH=8.0 buffered by $NaHCO_3$ was set as the electrolyte condition for the HAdV-2 solution

which was the same as in the hydrodynamic diameter measurements. All filtration experiments in this study were performed with the same hollow fiber. After each filtration experiment, the membrane was cleaned by filtering an aqueous solution of 0.01% sodium hypochlorite (NaOCl) and 5 mM ethylenediaminetetraacetic acid (EDTA) at the transmembrane pressure of 0.4 bar [32, 35]. The membrane permeate flux was recovered to that of the pristine membrane after the cleaning.

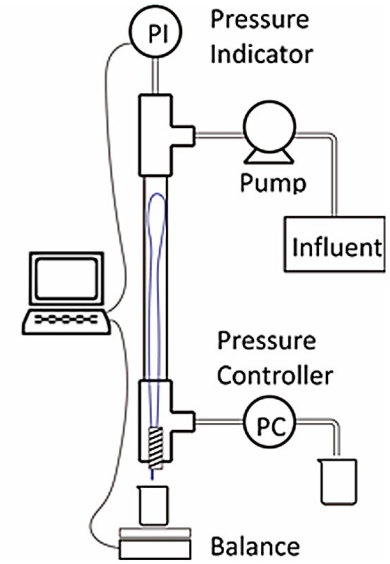

Figure 2.1 Schematic diagram of the single fiber microfiltration unit.

Virus removal and permeate flux were measured in filtration experiments with 3 different influent concentrations of HAdV-2: 1.3×10^7 copies/mL (low), 5.2×10^7 copies/mL (medium), and 3.4×10^8 copies/mL (high). Each filtration experiment included 4 steps. At Step 1 the membrane was conditioned with the background electrolyte solution in the absence of HAdV-2. Once the permeate flux decline was slower than 0.1×10^{-5} m/s within 30 min, the conditioning was stopped. Step 2 was filtration of the HAdV-2 solution for 50 min. The permeate samples were collected to calculate the log removal (LRV) of HAdV-2 by the membrane:

$$LRV = -log_{10}\frac{C_p}{C_f} \quad (1)$$

After the filtration step, the membrane surface was rinsed with the background electrolyte solution at zero transmembrane pressure (Step 3). During rinsing, the permeate flux was periodically tested with the background electrolyte solution at the transmembrane pressure of 0.4 bar. If the difference in the permeate flux within 3 continuous measurements was below 0.1×10^{-5} m/s, the rinsing was stopped. In Step 4 (referred to as "re-filtration") the HAdV-2 solution was filtered for another 50 min. The HAdV-2 removal and permeate flux during re-filtration were both recorded. For the high influent concentration, one more filtration experiment was done to ascertain whether HAdV-2 fouling occurred on the membrane surface or within membrane pores. The rinsing procedure (step 3 described above) was replaced by chemical rinsing of the membrane surface, while the other 3 steps remained unchanged. During the chemical rinsing, the transmembrane pressure was set at zero to avoid removing internal membrane foulant. The membrane surface was firstly rinsed with a 0.01% NaOCl solution for 30 min followed by 1 h of rinsing with deionized water. Afterwards, the membrane was rinsed with 5 mM EDTA solution at pH 11 for 30 min followed by a 1 h rinse with deionized water. The permeate flux after chemical cleaning was stabilized with the background electrolyte solution.

2.4 Model for HAdV-2 fouling microfiltration membrane

According to the combined pore blockage-cake filtration model [26], the permeate flux J as a function of time t is described by eq. (2):

$$J = J_0\left[\exp\left(-\frac{\alpha\Delta P C_b}{\mu R_m}t\right) + \frac{R_m\left(1-\exp\left(-\frac{\alpha\Delta P C_b}{\mu R_m}t\right)\right)}{(R_m+R_{p0})\sqrt{1+\frac{2f'R'\Delta P C_b}{\mu(R_m+R_{p0})^2}t}}\right] \quad (2)$$

where J_0 is the permeate flux through the pristine membrane, ΔP is the transmembrane pressure, C_b is the bulk concentration of foulant, and μ is the solution viscosity. The resistance of the pristine membrane R_m is given by eq. (3):

$$R_m = \frac{\Delta P}{\mu J_0} \quad (3)$$

The pore blockage parameter α, the resistance of a single foulant aggregate R_{p0}, and the increase rate of foulant layer resistance $f'R'$ are the 3 fitting parameters.

When using this model to explain HAdV-2 fouling the microfiltration membrane, the influent concentration of HAdV-2, C_f, was determined by qPCR in copies/mL, and thus

$$C_f = \frac{C_b}{M_v} \quad (4)$$

where the mass of each HAdV-2 particle M_v is 2.5×10^{-22} g [36]. The blockage parameter α is defined as:

$$\alpha = \frac{fA_v}{M_v} \quad (5)$$

where A_v is the area blocked by a single HAdV-2 particle and f is the fraction of HAdV-2 present as aggregates.

Using equations (2), (4), and (5), we derived an equation to fit the permeate flux as a function of time for HAdV-2 filtration:

$$J = J_0\left[\exp\left(-\frac{fA_v\Delta PC_f}{\mu R_m}t\right) + \frac{R_m\left(1-\exp\left(-\frac{fA_v\Delta PC_f}{\mu R_m}t\right)\right)}{(R_m+R_{p0})\sqrt{1+\frac{2M_v f' R' \Delta PC_f}{\mu(R_m+R_{p0})^2}t}}\right] \quad (6)$$

The fitting parameters for eq. (6) are fA_v, $f'R'$, and R_{p0}. In model fitting, ΔP was a constant of 0.4 bar or 4×10^4 Pa. C_b was the influent HAdV-2 concentration as mentioned above. The water viscosity μ at 25 ºC is 8.9×10^{-4} Pa·s.

2.5 Results and Discussion

Hydrodynamic diameter of HAdV-2. The measurement of the HAdV-2 hydrodynamic diameter in the 3 mM $CaCl_2$ solution at pH=8.0 showed a single peak at 175 ± 12 nm for 3 replicates. The half width at half maximum (HWHM) of the peak was 19 ± 1 nm, which was 11% of the peak of the hydrodynamic diameter. Additional replicate tests were run one day after the first measurement, and no statistically significant change of the hydrodynamic diameter was observed. These results indicated that HAdV-2 remained monodispersed in the ionic condition used in our filtration experiments. The measured value of the hydrodynamic diameter was

consistent with HAdV-2 structure studies, which indicated that HAdV-2 had an icosahedron capsid with 12 fibers projecting from the vertices of the capsid [23]. The capsid was reported to be 90 - 100 nm in diameter, and each fiber was 35-37 nm in length [37].

The HAdV-2 removal observed in microfiltration tests with different influent concentrations. The HAdV-2 removal kinetics for different influent concentrations are shown in Figure 2.2. For the influent with the lowest concentration, the HAdV-2 removal was highest at the very beginning and decreased over the first 30 min of filtration. For the next 20 min the removal remained statistically the same. A decrease of HAdV-2 removal at the beginning of filtration was also observed for the medium influent concentration. This trend in HADV-2 removal can be interpreted as resulting from virus adsorption by the membrane and virus diffusion across the membrane. Virus adsorption capacity is limited and contributes more to virus removal during very early stages of filtration. The early higher removals are likely due to continued adsorption. Rejected viruses tend to accumulate in the vicinity of the membrane surface, creating higher virus concentration gradient (ΔC) across the membrane. Given that HAdV-2 is smaller than the pore size, we expect that the convective transport of virus through the membrane is the dominant transport mechanism; however, ΔC-driven diffusive transport can also be a contributing factor, especially because of the small difference between the nominal pore size (200 nm) and the virus size (175 nm).

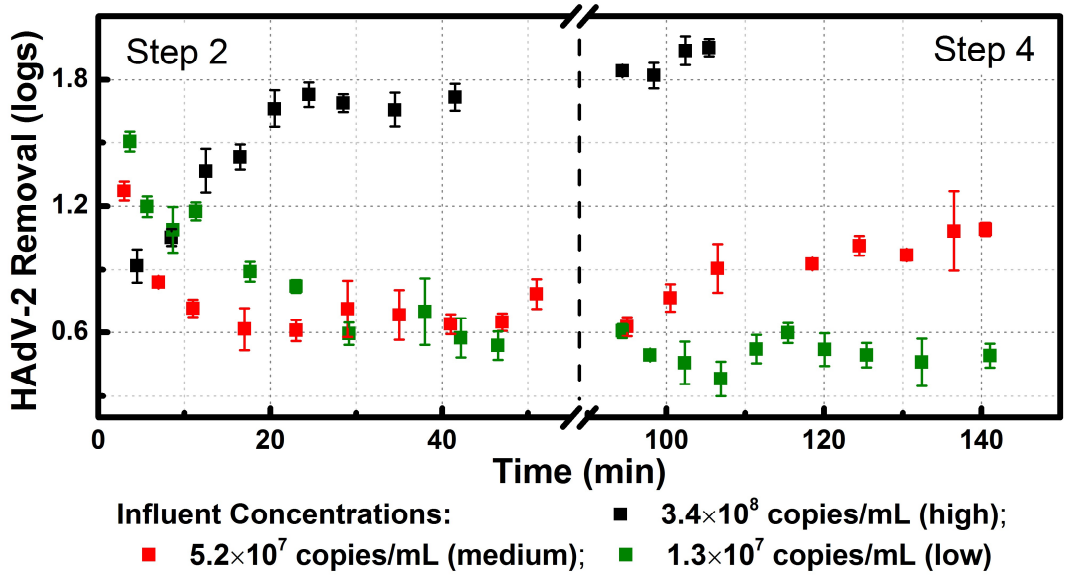

Figure 2.2 HAdV-2 removal over the filtration time in experiments with three different influent concentrations of the virus: 1.3×10^7 copies/mL (low; green squares), 5.2×10^7 copies/mL (medium; red squares), and 3.4×10^8 copies/mL (high; black squares). Error bars represent standard errors of triplicate permeate samples.

The accumulation of HAdV-2 on the membrane surface can be quantified in terms of the difference between virus concentrations at the membrane surface (C_m) and in the bulk of the feed (C_f). For the same intrinsic rejection R_i (eq. (7)), the observed rejection R_{obs}, (eq. (8)) is consequently lower when $\frac{C_m}{C_f}$ is higher:

$$R_i = 1 - \frac{C_p}{C_m} \tag{7}$$

$$R_i = 1 - \frac{C_p}{C_f} \tag{8}$$

At the later stages of filtration corresponding to cake filtration, C_m can be approximated by the concentration that corresponds to the random packing of viruses at the membrane surface. A simple calculation for HAdV-2 yields $C_m \approx 2.1\cdot10^{14}$ copies/mL. If one defines intrinsic log removal of viruses as

$$LRV_i = -\log_{10}\frac{C_p}{C_m} \tag{1a}$$

then

$$LRV_i = LRV + log_{10}\left(\frac{C_m}{C_f}\right). \tag{9}$$

For the influent concentration of $3.4\cdot10^8$ copies/mL (i.e., high influent concentration that may lead to cake filtration), $log_{10}\left(\frac{C_m}{C_f}\right) \approx 5.8$ and LRV of 1.8 (see Figure 2.2) translate to LRV_i of 7.6.

In the absence of a virus cake on the membrane surface, C_m is difficult to estimate. That is because the dependence of virus concentration on the distance from the cake-suspension interface is a complex function of virus-membrane interactions, as well as virus-virus interactions between viruses accumulation on the membrane surface.

In contrast to the trend observed for the low and medium influent concentrations, an increase in HAdV-2 removal over time was observed for the high influent concentration (Figure 2.2). For all three influent concentrations, the membrane rinse with the background electrolyte (see step 4 in Figure 2.2) did not alter virus removal. This finding suggested that HAdV-2 accumulated at the membrane surface could not be removed by simply rinsing with the electrolyte solution, and formed a hydraulically irreversible fouling layer.

To further understand why different trends of HAdV-2 removal kinetics were observed for different influent concentrations, we plotted the HAdV-2 removal as a function of the total number of HAdV-2 rejected by the membrane, N_r (Figure 2.3). The total number of HAdV-2 rejected by the membrane N_r was calculated using eq. 9:

$$N_r = \sum \left[\left(C_f - C_p\right) \Delta V\right], \quad (9)$$

where V is the total filtered volume. This equation assumes minimal back-transport of the virus away from the membrane surface. The assumption is justified because, in the effectively dead-end experiment, the only back-transport mechanism is diffusion, but the diffusivity of the HAdV2 is low. Indeed, as estimated using Stokes-Einstein's equation, the diffusivity at 25 ºC is $D = \frac{k_B T}{3\pi\mu d_p} = 2.5 \cdot 10^{-12}$ (m^2/s). This estimate is based on the virus size of 175 nm as measured by DLS, and assumes that the particle is spherical.

As shown in Figure 2.3, for $N_r < 10^9$ viral genome copies, a decrease of HAdV-2 removal with N_r was observed for the low influent concentration throughout step 2, and at the beginning of step 2 for the medium and high influent concentrations. This observed trend in HAdV-2 removal with N_r can be explained by the accumulation of HAdV-2 that was rejected by the membrane, as discussed above. With more HAdV-2 rejected by the membrane ($N_r >$

10^9 $virus$), an increase of the HAdV-2 removal with N_r can be explained by the formation of the fouling layer that contributed to the rejection.

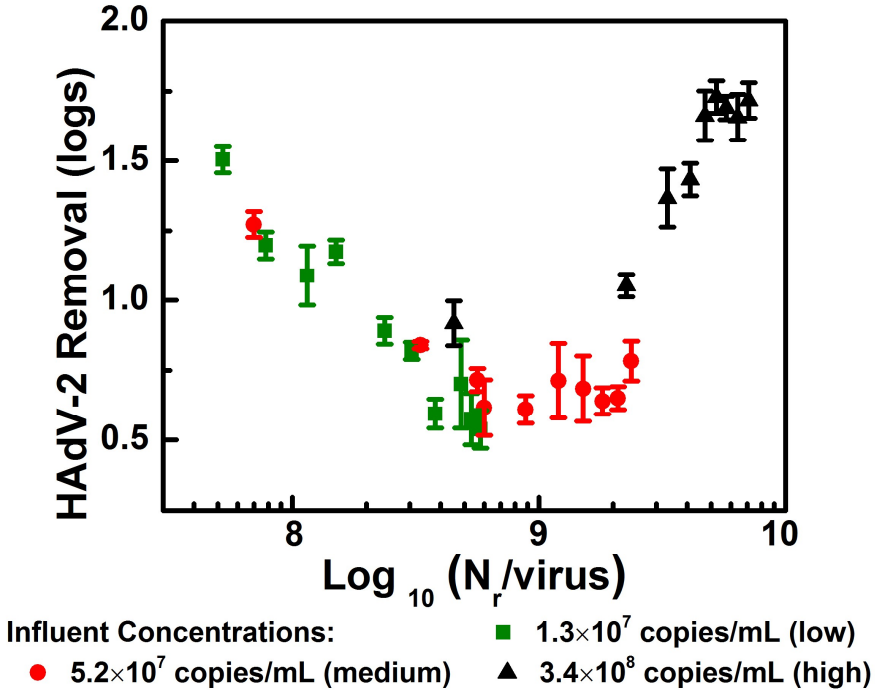

Figure 2.3 HAdV-2 removal as a function of the log value of the total number of rejected HAdV-2 (N_r). The data in step 2 of the filtration experiments are shown for 3 influent concentrations: low (green squares), medium (red circles), and high (black triangles).

The mechanisms of HAdV-2 fouling of the membrane can be determined by analyzing the permeate flux (Figure 2.4). The initial values of the permeate flux, J_0, for 3 influent concentrations were the same at 5.0×10^{-5} m/s. In step 2, the permeate flux for the low influent concentration did not decrease over the 50 min filtration. For the medium influent concentration, a gradual decrease was observed, while for the high influent concentration, a sharp decline in flux was followed by a slower continuing decrease. Rinsing the membrane with the electrolyte solution had none (for low and medium influent concentration) or minor (for high influent concentration) effects on the permeate flux (Figure 2.4), which was consistent with the observed lack of rinsing-induced changes in HAdV-2 removal (Figure 2.2). The fact that the permeate flux reaches (for high influent concentration) or approaches (for medium influent concentration)

steady state indicates that after the small pores of the microfilter are blocked, some large pores in the membrane stayed unblocked and were available for water and HAdV-2 permeation.

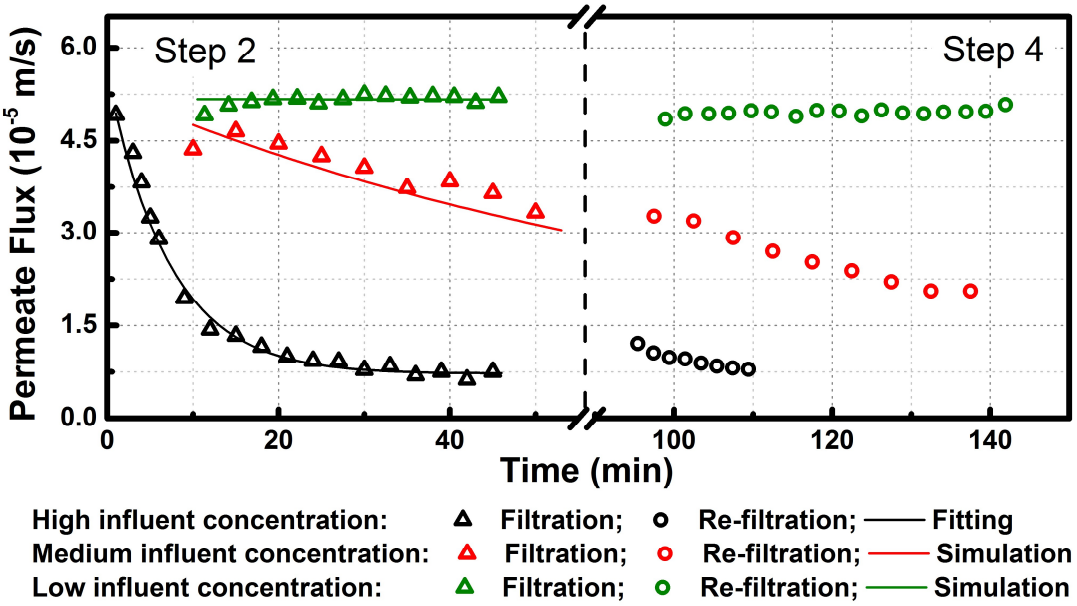

Figure 2.4 Permeate flux over filtration time for low (green), medium (red), and high (black) HAdV-2 influent concentration for both step 2 (hollow triangles) and step 4 (hollow circles).

Fouling mechanisms studied with the combined pore blockage-cake filtration (PB-CF) model. The PB-CF model [26] was applied to determine the mechanisms of HAdV-2 fouling of the membrane. The fitting curve for high influent concentration (Figure 2.4) had a coefficient of determination (R^2) of 0.97. The fitted parameters were: $fA_v = 1.16 \pm 0.02\times10^{-13}\ m^2/virus$, $R_{p0} = 5.8 \pm 0.5\times10^{12}\ m^{-1}$, and $R'_v = -2.4 \pm 4\times10^{20}\ m/g$. The resistance R_{p0} for HAdV-2 viruses was an order of magnitude higher than that of bovine serum albumin (BSA) aggregates reported in previous research ($4.0 \pm 0.2\times10^{11}\ m^{-1}$) [26]. The higher resistance of HAdV-2 than BSA aggregates was possibly due to the looser structure of BSA aggregates, which was formed by intermolecular disulfide bonds between albumin molecules [38]. The rate of increase in the HAdV-2 layer resistance $f'R'$ was not significantly different from 0, suggesting that the HAdV-2 layer resistance did not change with time. Because insignificant permeate flux decrease was observed for the low and medium influence concentration, fitting with the PB-CF model was not applicable. For these cases, the fitting parameters obtained in tests with the high influent

concentration were used to simulate the permeate flux as a function of filtration time for the medium and low influent concentrations. Note that the only difference among the three filtration experiments was the influent concentrations.

As shown in Figure 2.4, the simulation for the low and medium influent concentrations showed a good agreement with experimental data (R^2 of the simulations for low and medium influent concentrations are 0.86 and 0.95, respectively). The agreement between the fitted (high influent concentration) and simulated (low and medium influent concentration) curve with experimental results for the 3 influent concentrations verified that the PB-CF model can be used to explain the permeate flux decrease caused by HAdV-2 fouling.

To differentiate fouling mechanisms, the permeate flux data acquired from fitting (high influent concentration) or simulations (low and medium influent concentration) were plotted in $log_{10}\left(\frac{d^2t}{dV^2}\right)$ versus $log_{10}\left(\frac{dt}{dV}\right)$ to determine the slope n [26, 39, 40] (Figure 2.5).

$$\frac{dt}{dV} = \frac{1}{JA_m} \tag{12}$$

$$\frac{d^2t}{dV^2} = -\frac{1}{J^3A^2}\frac{dJ}{dt} \tag{13}$$

$\frac{dJ}{dt}$ was calculated using eq. (6). Theoretically, $n = 2$ means that the decrease of permeate flux is caused by complete pore blocking, $n = 1.5$ by standard blocking, n = 1 by intermediate blocking, and n = 0 for cake filtration [26].

The slopes at the beginning of filtration for low, medium, and high influent concentrations were 1.80, 1.84, and 1.75, respectively (Figure 2.5). The slope values between 1.5 and 2 suggest that a combination of complete blocking and standard blocking occurred at the beginning of filtration. In other words, HAdV-2 fouled the microfiltration membrane both on the membrane surface and within pores. For the low influent, n gradually decreased to 1.78 at the end of step 2. The little change of the slope n throughout step 2 for the low influent concentration indicated that membrane fouling was minimal, which was consistent with the stable flux observed (Figure 2.4). For the medium influent concentration, n decreased to 1.70 at the end of step 2. The decrease of this slope indicated that the dominant fouling mechanism transitioned from complete blocking to standard blocking. This transition was also observed for the case of BSA fouling of a microfiltration membrane [26]. We speculate that the non-uniform distribution of membrane

pore sizes could be the reason for the gradual decrease of n. Pores smaller than HAdV-2 were rapidly blocked at the beginning of filtration and were dominated by the complete blocking mechanism. With pores larger than HAdV-2 particles unblocked, a high fraction of permeate flux went through the unblocked pores. As filtration went on, HAdV-2 adsorbed on membrane pore channels and decreased the effective pore size. Therefore, standard blocking became more significant, and n became closer to 1.5 at the end of filtration for the medium influent concentration.

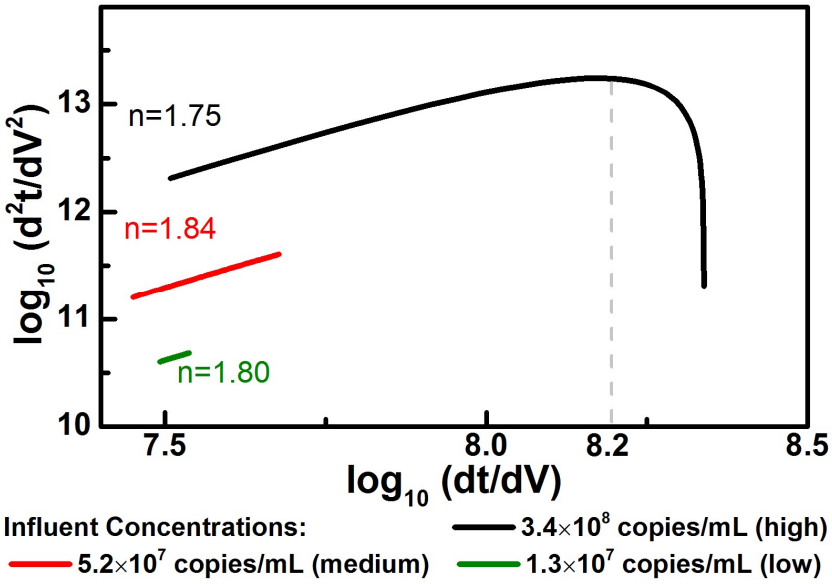

Figure 2.5 $log_{10}\left(\frac{d^2t}{dV^2}\right)$ as a function of $log_{10}\left(\frac{dt}{dV}\right)$ for 3 influent concentrations. For high influent (black), the data was calculated from the fitting curve of the experimental permeate flux. For low (green) and medium (red) influents, data was calculated from the simulation curves for the experimental permeate flux.

For the high influent concentration, the slope n gradually decreased to 0 at $log_{10}\left(\frac{dt}{dV}\right) = 8.2$ and kept decreasing sharply for $log_{10}\left(\frac{dt}{dV}\right) > 8.2$, as shown in Figure 2.5. The decrease of the slope n to 0 indicated that the capacity for pore blockage (complete blocking, standard blocking, and intermediate blocking) had been saturated and that a cake layer started to form. For $log_{10}\left(\frac{dt}{dV}\right) > 8.2$, n became negative. The negative n was also observed for BSA fouling

microfiltration membranes in previous studies [26, 41] and was interpreted as a transition from pore blockage to cake filtration. For BSA, a stable $n = 0$ was achieved as filtration went on, suggesting that cake layer became the dominant mechanism of membrane fouling over longer filtration times [26]. Although a stable $n = 0$ was not observed in HAdV-2 filtration after the decrease in step 2, the transition from pore blockage to cake layer formation was observed, indicating that the pores of the microfiltration membrane have been fully blocked by HAdV-2 both on the membrane surface (complete and intermediate blocking) and within membrane pores (standard blocking).

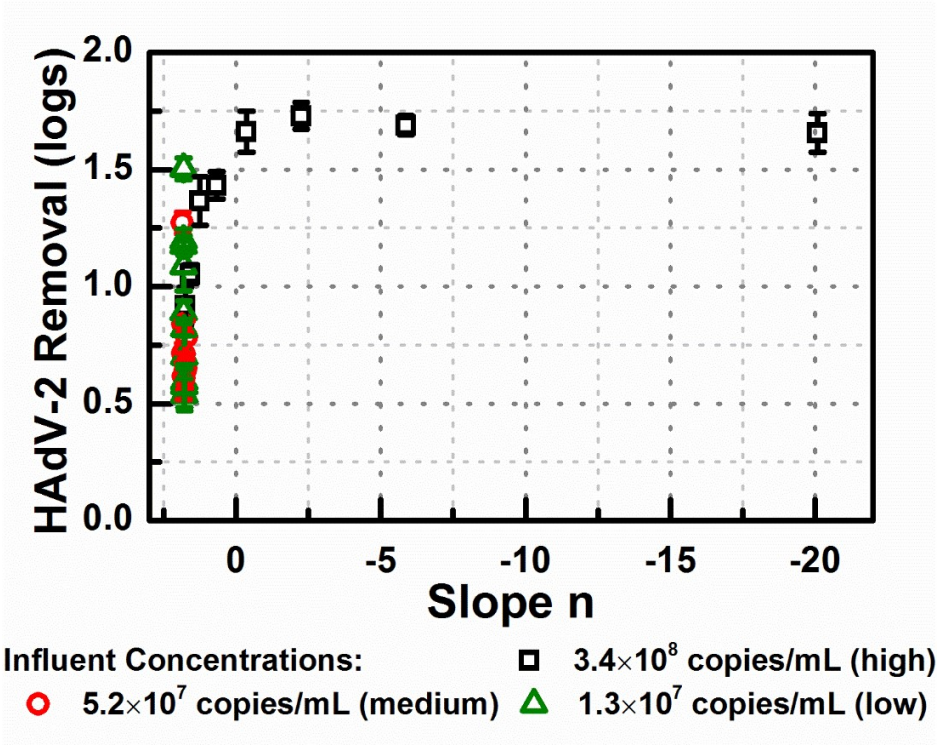

Figure 2.6 HAdV-2 removal as a function of the slope of $log_{10}\left(\frac{d^2t}{dV^2}\right)$ versus $log_{10}\left(\frac{dt}{dV}\right)$ for low (green), medium (red), and high (black) HAdV-2 influent concentrations in step 2.

The relationship between HAdV-2 removal and fouling mechanisms is analyzed by plotting the removal vs. the slopes (n) as determined from the data shown in Figure 2.6. For the high influent concentration, the HAdV-2 removal increased with the decrease of n for $n > 0$. With n decreasing to 0, most membrane pores were blocked by HAdV-2, and therefore fewer HAdV-2

could penetrate the membrane. For negative n, the membrane pores had been fully blocked by HAdV-2 allowing the formation of the cake layer, and the HAdV-2 removal did not show significant change with further decrease of n. For low and medium influent concentrations, the change of HAdV-2 removal occurred with n nearly unchanged, indicating that membrane fouling is not the dominant mechanism for the HAdV-2 removal change observed for the low and medium influent concentrations.

In summary, the modeling results showed that the increase of HAdV-2 removal with the total number of rejected HAdV-2 (N_r), the right half of Figure 2.3, is caused by HAdV-2 blocking the membrane pores while the decrease of HAdV-2 removal, the left half of Figure 2.3, is caused by the accumulation of rejected HAdV-2 on the membrane surface.

Contributions of internal and external fouling to HAdV-2 removal. The internal fouling is operationally defined here as components of the added hydraulic resistance due to fouling that can be removed by chemical cleaning with the cleaning solution filtered through the membrane. By contrast, the external fouling is defined as the added resistance that can be removed by flowing the chemical cleaning solution along the membrane surface at zero transmembrane pressure (i.e., in the absence of permeation). Both external and internal fouling could have contributed to the increase of HAdV-2 removal observed for the high influent concentration as shown in Figure 2.2. To distinguish between the contributions of internal and external foulants on HAdV-2 removal, the external foulant was removed by a chemical cleaning at zero transmembrane pressure in step 3. The permeate flux and HAdV-2 removal as functions of filtration time in steps 2 and 4 are shown in Figure 2.7. Only partial recovery of the permeate flux was observed after chemical cleaning of the membrane surface. The unrecovered portion of the permeate flux corresponds to internal fouling.

Similar to the results shown in Figure 2.2, HAdV-2 removal increased during step 2, as a result of HAdV-2 acting as the foulant (Figure 2.7). After the external chemical cleaning of the membrane surface, the HAdV-2 removal decreased by 0.5 log, indicating that the presence of external foulants contributed to the increase of virus removal. Comparing the HAdV-2 removal in steps 2 and 4 at the same permeate flux, the removal in step 4 was higher, suggesting that internal fouling might be more effective in enhancing HAdV-2 removal. Thus, our results prove

that a) HAdV-2 can cause both internal and external fouling of 0.2 um microfilter and that b) both types of fouling affect HAdV-2 removal.

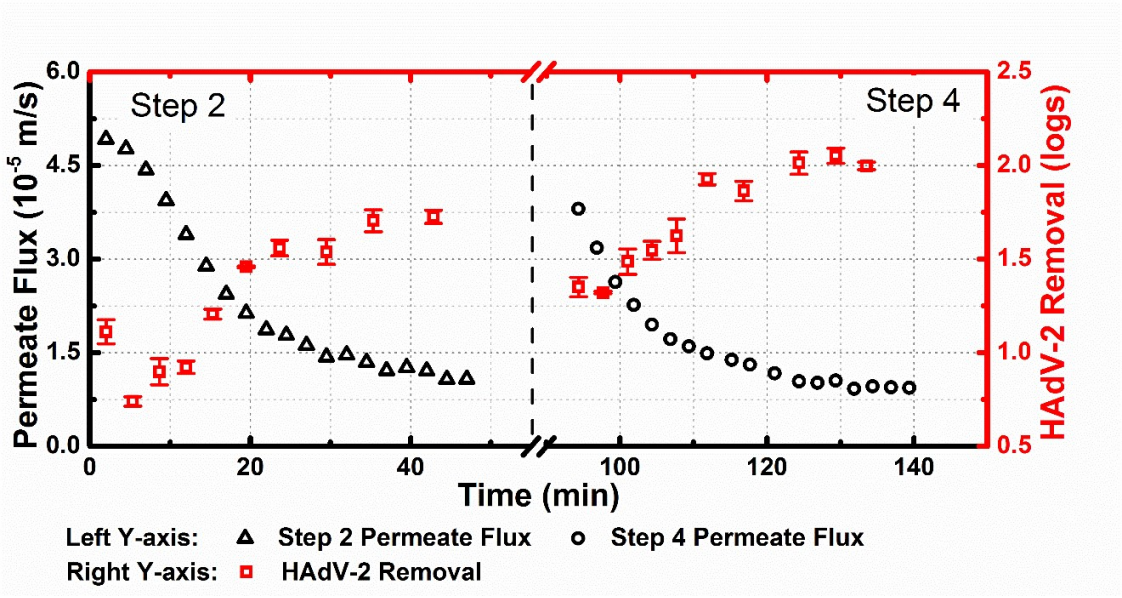

Figure 2.7 Effect of chemical removal of the external fouling on permeate flux and HAdV-2 removal in experiments with high influent concentration of HAdV-2, The permeate flux values plotted on the left Y-axis are shown as black hollow triangles (for Step 2) and as black hollow circles (for Step 4). Values of HAdV-2 removal (red squares) are plotted on the right Y-axis. Error bars represent the standard errors of triplicate permeate samples. External foulant was chemically cleaned in step 3.

2.6 Conclusions

The dynamics of HAdV-2 removal by a microfiltration membrane were illustrated in this study and the following general trends were observed:

- At the beginning of filtration, HAdV-2 rejected by the membrane accumulated in the vicinity of the membrane surface. The increase in C_m led to a decrease of the observed removal R_{obs} over the filtration time.

- At longer filtration times, HAdV-2 fouled the microfiltration membrane both internally and externally. The membrane pore blockage by HAdV-2 led to an increase of the observed HAdV-2 removal.
- Both external and internal fouling caused by HAdV-2 contributed to the increase in HAdV-2 removal and the decrease in permeate flux.

The results presented here can be useful for interpreting data on virus removal immediately after membrane cleaning when the fouling layer is minimal. In addition, the findings can also be beneficial for virus purification by membrane filtration in which only relatively pure virus suspensions are involved. For example, understanding the mechanisms of virus removal by porous membranes can help with the appropriate choice of membrane to minimize virus loss in the permeate, while enhancing impurities passing through the membrane.

Acknowledgements. The authors acknowledge the National Science Foundation for financial support in CBET Grant 1236672. We also acknowledge Nanxi Lv for inspiring discussions.

2.7 References

1. Cisneros, B.E.J., B. Jimenez, and T. Asano, *Water reuse: an international survey of current practice, issues and needs*. 2008: IWA Publishing.
2. USEPA, *Guidelines for Water Reuse, Office of Wastewater Management, Washington, DC. EPA/600/R-12/618.* 2012.
3. Mujeriego, R. and T. Asano, *The role of advanced treatment in wastewater reclamation and reuse.* Water Science and Technology, 1999. **40**(4): p. 1-9.
4. Fong, T.-T., et al., *Quantitative Detection of Human Adenoviruses in Wastewater and Combined Sewer Overflows Influencing a Michigan River.* Applied and Environmental Microbiology, 2010. **76**(3): p. 715-723.
5. Uhnoo, I., et al., *Importance of enteric adenoviruses 40 and 41 in acute gastroenteritis in infants and young children.* Journal of Clinical Microbiology, 1984. **20**(3): p. 365-372.
6. Xagoraraki, I., Z. Yin, and Z. Svambayev, *Fate of Viruses in Water Systems.* Journal of Environmental Engineering, 2014. **140**(7).

7. Simmons, F.J. and I. Xagoraraki, *Release of infectious human enteric viruses by full-scale wastewater utilities.* Water Research, 2011. **45**(12): p. 3590-3598.
8. Gander, M., B. Jefferson, and S. Judd, *Aerobic MBRs for domestic wastewater treatment: a review with cost considerations.* Separation and Purification Technology, 2000. **18**(2): p. 119-130.
9. Le-Clech, P., V. Chen, and T.A.G. Fane, *Fouling in membrane bioreactors used in wastewater treatment.* Journal of Membrane Science, 2006. **284**(1–2): p. 17-53.
10. van Dijk, L. and G.C.G. Roncken, *Membrane bioreactors for wastewater treatment: The state of the art and new developments.* Water Science and Technology, 1997. **35**(10): p. 35-41.
11. Kelly, S.T. and A.L. Zydney, *Mechanisms for BSA fouling during microfiltration.* Journal of Membrane Science, 1995. **107**(1–2): p. 115-127.
12. Yuan, W. and A.L. Zydney, *Humic acid fouling during microfiltration.* Journal of Membrane Science, 1999. **157**(1): p. 1-12.
13. Costa, A.R., M.N. de Pinho, and M. Elimelech, *Mechanisms of colloidal natural organic matter fouling in ultrafiltration.* Journal of Membrane Science, 2006. **281**(1–2): p. 716-725.
14. Eshet, I., et al., *Chemical and Physical Factors in Design of Antibiofouling Polymer Coatings.* Biomacromolecules, 2011. **12**(7): p. 2681-2685.
15. Herzberg, M., et al., *Surface Properties and Reduced Biofouling of Graft-Copolymers That Possess Oppositely Charged Groups.* Biomacromolecules, 2011. **12**(4): p. 1169-1177.
16. Kang, S., et al., *Protein antifouling mechanisms of PAN UF membranes incorporating PAN-g-PEO additive.* Journal of Membrane Science, 2007. **296**(1-2): p. 42-50.
17. Liang, S., et al., *Highly Hydrophilic Polyvinylidene Fluoride (PVDF) Ultrafiltration Membranes via Postfabrication Grafting of Surface-Tailored Silica Nanoparticles.* ACS Applied Materials & Interfaces, 2013. **5**(14): p. 6694-6703.
18. Liang, S., et al., *Organic fouling behavior of superhydrophilic polyvinylidene fluoride (PVDF) ultrafiltration membranes functionalized with surface-tailored nanoparticles: Implications for organic fouling in membrane bioreactors.* Journal of Membrane Science, 2014. **463**: p. 94-101.

19. Mauter, M.S., et al., *Antifouling Ultrafiltration Membranes via Post-Fabrication Grafting of Biocidal Nanomaterials.* Acs Applied Materials & Interfaces, 2011. **3**(8): p. 2861-2868.
20. Urase, T., K. Yamamoto, and S. Ohgaki, *Effect of pore structure of membranes and module configuration on virus retention.* Journal of Membrane Science, 1996. **115**(1): p. 21-29.
21. Farahbakhsh, K. and D. Smith, *Removal of coliphages in secondary effluent by microfiltration—mechanisms of removal and impact of operating parameters.* Water Research, 2004. **38**(3): p. 585-592.
22. Zodrow, K., et al., *Polysulfone ultrafiltration membranes impregnated with silver nanoparticles show improved biofouling resistance and virus removal.* Water Research, 2009. **43**(3): p. 715-723.
23. Horwitz, M.S., *Adenoviruses.* Fields virology, 2001. **2**: p. 2301-2326.
24. Hong, S., R.S. Faibish, and M. Elimelech, *Kinetics of permeate flux decline in crossflow membrane filtration of colloidal suspensions.* Journal of Colloid and Interface Science, 1997. **196**(2): p. 267-277.
25. Chen, V., et al., *Particle deposition during membrane filtration of colloids: transition between concentration polarization and cake formation.* Journal of Membrane Science, 1997. **125**(1): p. 109-122.
26. Ho, C.C. and A.L. Zydney, *A Combined Pore Blockage and Cake Filtration Model for Protein Fouling during Microfiltration.* J Colloid Interface Sci, 2000. **232**(2): p. 389-399.
27. Tracey, E.M. and R.H. Davis, *Protein fouling of track-etched polycarbonate microfiltration membranes.* Journal of Colloid and Interface Science, 1994. **167**(1): p. 104-116.
28. Pina, S., et al., *Viral Pollution in the Environment and in Shellfish: Human Adenovirus Detection by PCR as an Index of Human Viruses.* Applied and Environmental Microbiology, 1998. **64**(9): p. 3376-3382.
29. Kuo, D.H.W., et al., *Assessment of human adenovirus removal in a full-scale membrane bioreactor treating municipal wastewater.* Water Research, 2010. **44**(5): p. 1520-1530.

30. Kim, K.-J., V. Chen, and A.G. Fane, *Ultrafiltration of colloidal silver particles: flux, rejection, and fouling.* Journal of Colloid and Interface Science, 1993. **155**(2): p. 347-359.
31. Sirikanchana, K., J.L. Shisler, and B.J. Mariñas, *Effect of exposure to UV-C irradiation and monochloramine on adenovirus serotype 2 early protein expression and DNA replication.* Applied and Environmental Microbiology, 2008. **74**(12): p. 3774-3782.
32. Lu, R., D. Mosiman, and T.H. Nguyen, *Mechanisms of MS2 Bacteriophage Removal by Fouled Ultrafiltration Membrane Subjected to Different Cleaning Methods.* Environmental Science & Technology, 2013. **47**(23): p. 13422-13429.
33. Pham, M., E.A. Mintz, and T.H. Nguyen, *Deposition kinetics of bacteriophage MS2 to natural organic matter: Role of divalent cations.* Journal of Colloid and Interface Science, 2009. **338**(1): p. 1-9.
34. Heim, A., et al., *Rapid and quantitative detection of human adenovirus DNA by real-time PCR.* Journal of Medical Virology, 2003. **70**(2): p. 228-239.
35. Sweity, A., et al., *pH effects on the adherence and fouling propensity of extracellular polymeric substances in a membrane bioreactor.* Journal of Membrane Science, 2011. **378**(1-2): p. 186-193.
36. Van Oostrum, J. and R.M. Burnett, *Molecular composition of the adenovirus type 2 virion.* Journal of Virology, 1985. **56**(2): p. 439-448.
37. Devaux, C., et al., *Structure of adenovirus fibre: I. Analysis of crystals of fibre from adenovirus serotypes 2 and 5 by electron microscopy and X-ray crystallography.* Journal of Molecular Biology, 1990. **215**(4): p. 567-588.
38. Kelly, S.T. and A.L. Zydney, *Effects of intermolecular thiol–disulfide interchange reactions on BSA fouling during microfiltration.* Biotechnology and bioengineering, 1994. **44**(8): p. 972-982.
39. Hermans, P. and H. Bredée, *Principles of the mathematical treatment of constant-pressure filtration.* J. Soc. Chem. Ind, 1936. **55**: p. 1-4.
40. Gonsalves, V., *A critical investigation on the viscose filtration process.* Recueil des Travaux Chimiques des Pays-Bas, 1950. **69**(7): p. 873-903.
41. Bowen, W., J. Calvo, and A. Hernandez, *Steps of membrane blocking in flux decline during protein microfiltration.* Journal of Membrane Science, 1995. **101**(1): p. 153-165.

CHAPTER 3

RANDOM SEQUENTIAL ADSORPTION OF HUMAN ADENOVIRUS 2 ONTO POLYVINYLIDENE FLUORIDE SURFACE INFLUENCED BY EXTRACELLULAR POLYMERIC SUBSTANCES

Published in *Journal of Colloid and Interface Science*, 2016

Lu, R., Q. Li, and T.H. Nguyen, *Random sequential adsorption of human adenovirus 2 onto polyvinylidene fluoride surface influenced by extracellular polymeric substances*. Journal of Colloid and Interface Science, 2016. **466**: p. 120-127.

3.1 Abstract

Virus removal by membrane bioreactors depends on virus-membrane and virus-foulant interactions. The adsorption of human adenovirus 2 (HAdV-2) on polyvinylidene fluoride (PVDF) membrane and a major membrane foulant, extracellular polymeric substances (EPS), were measured in a quartz crystal microbalance. In 3 mM to 100 mM $CaCl_2$ solutions, irreversible adsorption of HAdV-2 was observed on both pristine and EPS-fouled PVDF surfaces. The HAdV-2 adsorption kinetics was successfully fitted with the random sequential adsorption (RSA) model. The applicability of the RSA model for HAdV-2 adsorption is confirmed by comparing the two fitting parameters, adsorption rate constant k_a and area occupied by each adsorbed HAdV-2 particle a, with experimentally measured parameters. A linear correlation between the fitting parameter k_a and the measured attachment efficiency was found, suggesting that the RSA model correctly describes the interaction forces dominating the HAdV-2 adsorption. By comparing the fitting parameter d_{ads} with the hydrodynamic diameter of HAdV-2, we conclude that virus-virus and virus-surface interactions determine the area occupied by each adsorbed HAdV-2 particle, and thus influence the adsorption capacity. These results provide insights into virus retention and will benefit improving virus removal in membrane filtration.

3.2 Introduction

In the context of increasing water demand in many countries including the United States, municipal wastewater reuse has been proposed as an effective approach to increase the water supply [1]. Though non-potable reuse of municipal wastewater has been in practice, safety issues, especially microbial safety, are the major concern of water consumers [2]. Among pathogens in wastewater, special attention has been paid to viruses because of their low-dose infectivity [3], long survival time in the environment [4], and the lack of systematic monitoring [5].

Compared to conventional processes, membrane bioreactors (MBR) have the potential to achieve higher virus removal and to ensure public safety in wastewater reuse [6-8]. Investigation of virus removal by MBR found that pristine membranes alone achieved relatively low virus removal, while membrane foulants greatly increased the virus removal efficiency [9-11]. However, virus removal by a fouled membrane is energy-intensive and unstable [10]. The necessity of developing anti-fouling membranes with a high virus removal efficiency has been highlighted [12]. One of the obstacles to developing these membranes is the lack of knowledge on virus behavior at the water-membrane interface. Previous research of virus adsorption on or elution from membranes focused on the mechanism of virus-membrane interaction forces [13-16]. For oppositely charged virus and membranes, the attractive electrostatic force dominates virus adsorption. In the condition that virus and membranes are both negatively charged, electrostatic interaction, hydrophobic interaction, and salt bridges jointly determine the virus adsorption onto membranes.

Knowledge of interaction forces is significant but not sufficient to predict virus behavior on membrane surfaces, especially in the aspect of adsorption kinetics and capacity. The kinetics of virus adsorption onto the membrane influences the virus removal both directly and indirectly. The direct influence is that there are less adsorption sites available as the filtration goes on, resulting in a decrease of virus removal over the filtration time. The indirect influence is that the viruses adsorbed to the membrane will decrease the effective membrane pore size and even completely block the pores, leading to an increase of the virus removal. With these two mechanisms, virus adsorption influences the dynamics of virus removal both in the short-term and long-term membrane filtration [17-19]. Therefore, a quantitative understanding of virus

adsorption kinetics onto membranes is required to predict the virus removal efficiency by membrane filtration.

The random sequential adsorption (RSA) model has been shown to be applicable in explaining the adsorption of colloids and proteins [20-26]. According to the RSA model, an incoming particle adsorbs onto the surface at a random position if there is no overlap with previously adsorbed particles. The adsorption site on the surface is assumed to be continuous, unlike the assumption of discrete adsorption sites in the Langmuir model. Considering that the size of viruses is larger than 20 nm, and that the distance between adsorption sites on membrane surfaces is much smaller, the RSA model is closer to the nature of virus adsorption than the Langmuir model. A better prediction of colloid adsorption with RSA than Langmuir has been validated, especially in the range of high surface coverage [22, 26]. The RSA model is applied in this work to investigate the virus adsorption kinetics and capacity onto membrane surfaces.

The specific objective of this work is to quantitatively investigate the virus adsorption onto the polyvinylidene difluoride (PVDF) membrane with the adsorbed mass measured in real time using a quartz crystal microbalance with dissipation (QCM-D). Human adenovirus 2 (HAdV-2) is used as a model virus because human adenovirus has been suggested to be an indicator of human viruses due to its high detection frequency in wastewater, and also because of its virulence causing respiratory and diarrhea diseases [27-29]. PVDF is one of the most commonly used materials for micro- and ultrafiltration membranes in the MBR market because of its excellent chemical, thermal, and mechanical properties [30, 31]. Since membrane foulants in MBR influence membrane surface properties, the effect of a major MBR foulant, extracellular polymeric substances (EPS) [32-34], on HAdV-2 adsorption is also discussed in this study.

3.3 Methods and materials

HAdV-2 propagation. The HAdV-2 (ATCC, VR-846) used in this study was propagated in the A549 human lung carcinoma cells (Diagnostic Hybrids). The A549 cells were propagated at 37 ℃ in 5% CO_2 with Ham's F12K growth media supplemented with 10% fetal bovine serum (FBS), 100 U/ml of penicillin, 100 µg/ml of streptomycin, and 0.25 µg/ml of amphotericin B [35]. Right after a full confluence on the flask, the A549 cells were inoculated with HAdV-2.

The media for HAdV-2 propagation was supplemented with 2% FBS, with other components the same as the A549 cell propagation media. After the cytopathic effect of the cells was observed, the flask was repeatedly frozen at -80 ℃ and thawed at 4 ℃ for 3 cycles. The cell debris was removed by centrifuging the suspension at 230×g for 10 minutes, and then filtering the supernatant with a 0.45 μm pore size membrane (Corning CLS431155). The filtrate was transferred to an Amicon stirred cell (Millipore), and the HAdV-2 was retained in the stirred cell with a 100 kDa ultrafiltration membrane (Koch HFM-180), while impurities smaller than 100 kDa were washed away by a 1mM $NaHCO_3$ solution. The finished HAdV-2 stock concentration was quantified with the quantitative real-time PCR (qPCR) method, as described in our previous study [19].

EPS extraction from a full scale MBR. The full scale MBR activated sludge sample was collected from Traverse City Wastewater Treatment Plant (Michigan). EPS was extracted from the activated sludge with formaldehyde and NaOH [36]. Specifically, the biomass was precipitated by centrifuging 20 mL of the activated sludge at 5,000 g for 30 minutes, and the supernatant was discarded. After rinsing the biomass with 0.85% NaCl solution to remove the supernatant residues, the biomass was resuspended into a 10 mL 0.85% NaCl solution. 120 μL of 36% formaldehyde was added to the suspension, and the mixture was shaken gently at 4 °C for one hour. Afterwards, 8 mL of 1 M NaOH was added and the sample was shaken gently at 4 °C for an additional three hours. By centrifuging at 20,000 g for 30 minutes at 4 °C, extracted EPS was separated from the biomass and was in the supernatant. Solids in the supernatant were filtered with a 0.2 μm membrane. NaOH and formaldehyde in the filtrate were removed with a 3,500 MWCO dialysis membrane (Thermo Scientific). The dialysis was complete when the conductivity of the buffer water in equilibrium was below 15 μS/cm. Dialyzed EPS went through lyophilization and was stored at -20 °C.

Hydrodynamic diameter and electrophoretic mobility of HAdV-2 and EPS. The hydrodynamic diameter and electrophoretic mobility (EPM) of HAdV-2 were examined with a Zetasizer ZS90 (Malvern, UK) at the wavelength of 633 nm and the scattering angle of 90°. The hydrodynamic diameter measurements were conducted in $CaCl_2$ solutions from 1 to 100 mM, and the pH was adjusted to 8.0 with $NaHCO_3$. For each $CaCl_2$ concentration, three replicate samples were examined right after sample preparation, and each replicate was examined again 24

hours after preparation to investigate the aggregation of HAdV-2. The isoelectric point (IEP) of HAdV-2 was determined by measuring the electrophoretic mobility (EPM) of HAdV-2 in 3mM $CaCl_2$ solution at pH from 3.0 to 8.9, which was adjusted with 10 mM HCl or NaOH. The EPM of HAdV-2 and EPS in 1 to 100 mM $CaCl_2$ solutions were measured at pH = 8.0. Three replicates were examined for each condition. The surface potentials of HAdV-2 and EPS were calculated from EPM following Ohshima's method [37-39]. The concentration of HAdV-2 in the hydrodynamic diameter and EPM measurements was 5×10^7 virus/mL by q-PCR, and the concentration of the EPS was 160 mg/L.

Proton nuclear magnetic resonance (^{1}H-NMR) of the extracted EPS. The ^{1}H-NMR spectra of extracted EPS was measured with a VARIAN UNITY INOVA 600 MHz NMR system equipped with a 5 mm Varian AutoTuneX 1H/X PFG Z probe. The lyophilized EPS was dissolved into the 99.9% deuterium oxide (Sigma-Aldrich) at a concentration of 640 mg/L. pH of the EPS solution was adjusted to 8.0 with sodium deuteroxide (Sigma-Aldrich). The spectrum was acquired with 14050 scans using a sweep width of 8000 Hz at a spectrometer frequency of 600 MHz.

HAdV-2 adsorption onto pristine and EPS-fouled PVDF studied with QCM-D. A QCM-D 300 system (Biolin Scientific, Sweden) was applied to study the HAdV-2 adsorption to the pristine and EPS-fouled PVDF surfaces. The PVDF sensors (QSX-999) were supplied by Biolin Scientific (Sweden) by spin coating PVDF onto the gold sensors with a fundamental resonant frequency 5 MHz (Biolin Scientific, Sweden). The thickness of the coated PVDF layer was 50 nm as reported by the manufacturer. The roughness of the PVDF surface was determined to be around 2 nm using AFM in the tapping mode. The same sensor has been used to represent the PVDF membranes in previous studies [40, 41]. The flow rate in the QCM-D chamber was fixed at 0.1 mL/min, and the corresponding Reynolds number was 1.0. The frequency and dissipation shift of the sensor (Δf and ΔD, respectively) were both monitored as a function of time. Before each adsorption experiment, the baseline of the sensor was established with degassed deionized (DI) water until the flocculation of frequency shift was less than 0.1 Hz within 30 minutes.

The HAdV-2 adsorption onto the pristine and EPS-fouled PVDF surfaces was investigated in four $CaCl_2$ concentrations: 3 mM, 10 mM, 30 mM, and 100 mM. In all adsorption experiments, pH was adjusted to 8.0. For HAdV-2 adsorption onto the pristine PVDF, the sensor was

equilibrated with the $CaCl_2$ solution for 20 min after establishing the baseline with DI water. Following the equilibration, HAdV-2 (7.5×10^7 copies/mL) in the $CaCl_2$ solution was pumped into the QCM-D chamber to determine the change of Δf and ΔD. The HAdV-2 adsorption lasted for 40 minutes, and afterwards the virus free $CaCl_2$ solution was flowed into the chamber to investigate the reversibility of HAdV-2 adsorption. For HAdV-2 adsorption onto the EPS-fouled PVDF surface, the equilibration with the $CaCl_2$ solution was the same as that for the pristine PVDF surface. Afterwards, EPS was adsorbed to PVDF by flowing the EPS solution at a concentration of 160 mg/L in 3 mM $CaCl_2$ for 1 hour. The unbound EPS was washed away by the 3 mM $CaCl_2$ solution. The EPS-fouled PVDF sensor was equilibrated with the same $CaCl_2$ solution to be used for the subsequent HAdV-2 adsorption. The HAdV-2 adsorption onto the EPS-fouled PVDF surface also lasted for 40 minutes, followed by the virus free $CaCl_2$ solution to determine the reversibility of HAdV-2 adsorption.

The attachment efficiency α of HAdV-2 onto the pristine and EPS-fouled PVDF is calculated from the frequency shift at the 3rd overtone Δf_3 with the equation [42, 43]:

$$\alpha = \frac{(\frac{d\Delta f_3}{dt})_{t\to0}}{(\frac{d\Delta f_3}{dt})_{t\to0,fav}} \quad (1)$$

where $(\frac{d\Delta f_3}{dt})_{t\to0}$ is the rate of Δf_3 change over time at the very beginning of HAdV adsorption onto the pristine and EPS-fouled PVDF surfaces, and $(\frac{d\Delta f_3}{dt})_{t\to0,fav}$ is that of HAdV adsorption in the favorable condition. The favorable HAdV-2 adsorption was achieved by coating the positively charged poly-L-lysine (PLL) (Sigma-Aldrich, MO) onto a silica sensor (QSX 303, Q-sense) [43, 44]. 2 mL PLL hydrobromide solution (0.1 g/L PLL hydrobrimide in HEPES buffer) was flowed through the chamber, and the excess PLL was washed away with HEPES buffer. The HEPES buffer was made with 10 mM *N*-(2-hydroxyethyl) piperazine-*N'*-2-ethanesulfonic acid and 100 mM NaCl. Before HAdV-2 adsorption, the PLL layer was equilibrated with the same $CaCl_2$ solution to be used for the subsequent HAdV-2 adsorption. By flowing a 7.5×10^7 virus/mL (by qPCR) HAdV-2 solution to the PLL surface, the rate of Δf_3 change over time at the very beginning of HAdV-2 favorable adsorption $(\frac{d\Delta f_3}{dt})_{t\to0,fav}$ was determined.

The RSA model description. An equation to describe the kinetics of RSA has been developed [45-47]:

$$\frac{d\Gamma}{dt} = mk_a C_b[1 + 0.812\frac{\Gamma a}{m\theta_\infty} + 0.4258\left(\frac{\Gamma a}{m\theta_\infty}\right)^2 + 0.0716\left(\frac{\Gamma a}{m\theta_\infty}\right)^3](1 - \frac{\Gamma a}{m\theta_\infty})^3 \qquad (2)$$

in which Γ is the surface mass density and t is time. The adsorption rate constant k_a is the product of attachment efficiency α and particle transfer coefficient K, which characterizes the kinetics of the capture of suspended colloidal particles by bare collectors [26].

$$k_a = \alpha K \qquad (3)$$

C_b is the particle concentration (count per volume) in the bulk solution. a is the area occupied by each adsorbed particle on the surface, and m is the particle mass. For HAdV-2 adsorption onto PVDF, the bulk concentration of HAdV-2, C_b, was determined to be 7.5×10^7 virus/mL by q-PCR, and the mass of a single HAdV-2 particle m has been reported to be $2.47\times10^{-7}\ ng$ [48]. $\theta_\infty = 0.547$ is the maximum coverage of hard, non-interacting particles [49]. The surface mass density Γ was calculated from Δf_3 measured by QCM-D, with the Sauerbrey equation [50]:

$$\Gamma = -\frac{c}{3}\Delta f_3 \qquad (4)$$

where c is a constant of 17.7 $ng/(cm^2\ Hz)$. The adsorption rate constant k_a and the area occupied by each adsorbed HAdV-2 particle a were determined by fitting QCM-D data with equation 2.

3.4 Results and discussion

Characterization of HAdV-2 and EPS. The hydrodynamic diameter of HAdV-2 in 1 to 100 mM $CaCl_2$ solutions is shown in Figure 3.1 (a). In all the $CaCl_2$ solutions tested, the hydrodynamic diameter of HAdV-2 is between 171 and 178 nm. Results here are consistent with previous research on the structure of HAdV-2 [51, 52], which indicates that the HAdV-2 capsid is an icosahedron (~ 90 nm in diameter) with fibers (~ 37 nm meter in length) projecting from the 12 vertices. The results of hydrodynamic diameter measurement suggest that HAdV-2 was mono-dispersed in all the $CaCl_2$ solutions tested. The hydrodynamic diameter of HAdV-2 did not change within 24 hours, suggesting that no aggregation occurred.

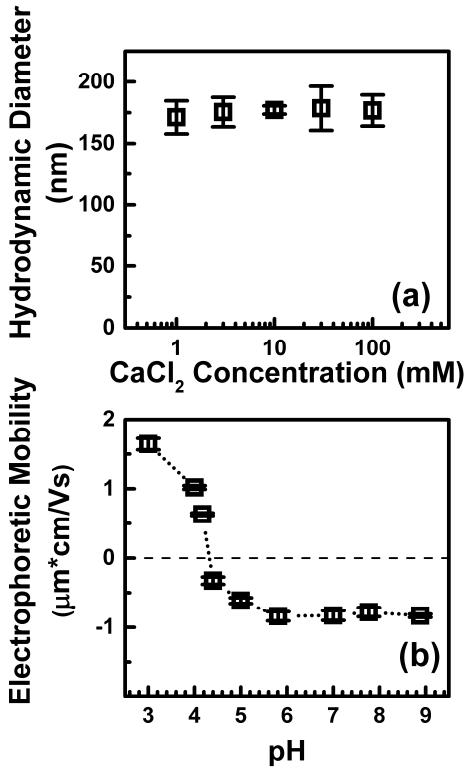

Figure 3.1 (a) The hydrodynamic diameter of HAdV-2 in 1 – 100 mM $CaCl_2$ solutions at pH=8.0; (b) The electrophoretic mobility of HAdV-2 at pH from 3.0 to 8.9.

Based on the measured EPM of HAdV-2 at different pH as shown in Figure 3.1 (b), the IEP of HAdV-2 is found to be 4.3. Although the IEP of HAdV-2 has not been reported, HAdV-5 is in the same species as HAdV-2, and its IEP of 4.5 is close to our measurement [53]. The EPM and surface potential of HAdV-2 and EPS in different $CaCl_2$ concentrations at pH = 8.0 are shown in Table 3.1. For HAdV-2 and EPS in 1 to 100 mM $CaCl_2$ solutions, the EPMs are negative and become less negative with increasing $CaCl_2$ concentration due to the charge shielded by Ca^{2+}. The surface charge of the PVDF sensors used in the adsorption experiments was not measured in this study. However, previous research found that the charge of PVDF was close to 0 even in a low ionic strength (around -3 mV in 5 mM KNO_3 or similar solutions) [54-56]. Since the HAdV-2 adsorption experiments in this study were conducted in higher ionic strength, the charge of the PVDF sensors would be close to 0.

Table 3.1 Electrophoretic mobility and surface potential of HAdV-2 and EPS for various $CaCl_2$ concentrations (pH = 8.0, T = 298 K).

$CaCl_2$ Concentration (mM)	HAdV-2		EPS	
	Electrophoretic Mobility (μm cm/Vs)	Surface Potential* (mV)	Electrophoretic Mobility (μm cm/Vs)	Surface Potential* (mV)
1	-1.43±0.07	-12.22	-0.82±0.08	-5.58
3	-0.88±0.01	-3.91	-0.49±0.06	-1.70
10	-0.60±0.06	-1.31	-0.35±0.06	-0.57
30	-0.43±0.08	-0.44	-0.32±0.04	-0.19
100	-0.13±0.06	-0.13	-0.23±0.03	-0.06

* The surface potentials were calculated with Ohshima's method [37-39].

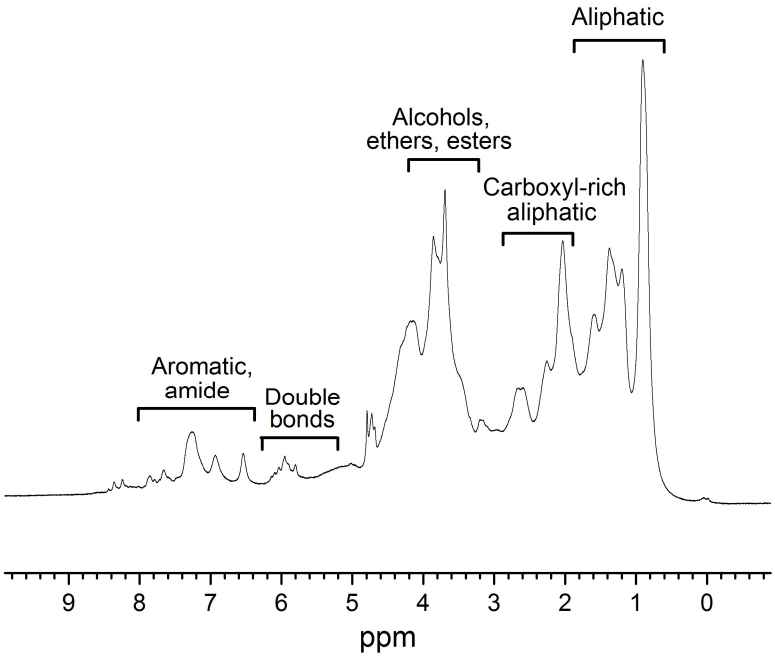

Figure 3.2 ^{1}H-NMR spectra of EPS extracted from the activated sludge in a full scale MBR.

To interpret the HAdV-2 adsorption onto the EPS-fouled PVDF surface, it is necessary to know the composition of EPS extracted from the full scale MBR. The ^{1}H-NMR spectra of extracted EPS is shown in Figure 3.2. The major bands of resonance are between 0 to 5 ppm, which indicates that most protons are in the aliphatic region, while the minor peaks with resonance between 6 and 8.6 indicate the presence of aromatic compounds [57]. In accordance with the previous ^{1}H-NMR spectra results of natural organic matters [58-60], peaks from 0.5 to 1.8 ppm are the resonance of aliphatic methyl and methylene protons; 1.8 to 2.5 ppm are protons in amine groups, α-carbons in ester groups, carboxylic groups, and carbonyl groups; 3.5 to 4.8 ppm can be attributed to protons on alcohols, ethers, esters, and haloalkanes. The minor peaks in the aromatic region are in the range of 5.6 to 8 ppm and can correspond to amides, quinones, and phenols. The ^{1}H-NMR spectra peak distribution of EPS extracted in this work is close to Suwanee River fulvic acid and Nordic fulvic acid but not similar to the spectra of humic acids [59]. Therefore, the extracted EPS might consist of relatively low molecular weight and high oxygen content [61].

HAdV-2 adsorption onto the pristine and EPS-fouled PVDF surfaces. The HAdV-2 adsorption was investigated with the QCM-D. The steps of HAdV-2 adsorption onto (a) PLL, (b) pristine PVDF, and (c) EPS-fouled PVDF in 3 mM $CaCl_2$ solution is shown in Figure 3.3, with Δf_3 in the left axis and ΔD_3 in the right axis. The dissipation shift of HAdV-2 adsorption onto PLL in 3 mM $CaCl_2$ solution was the largest within all the QCM-D experiments. Since the dissipation shift in all experiments are smaller than 3×10^{-6}, we assume that the adsorbed HAdV-2 layer is rigid, and thus the Sauerbrey equation was used to calculate the surface mass density Γ [46, 62]. For all surfaces studied, as shown in Figure 3.3, Δf_3 decreased quickly at the beginning of the HAdV-2 adsorption step, and the decrease became slower as the adsorption went on. The slower decrease of Δf_3 may be attributed to the monolayer adsorption of HAdV-2. After the step of HAdV-2 adsorption, the surface was rinsed with HAdV-2 free $CaCl_2$ solutions to determine the reversibility of HAdV-2 adsorption. There is no significant change in Δf_3 during the rinsing step, suggesting irreversible HAdV-2 adsorption onto PLL and pristine/EPS-fouled PVDF surfaces. In 10 mM, 30 mM, and 100 mM $CaCl_2$ solutions, the decreasing adsorption rate and the irreversible adsorption of HAdV-2 were also observed. The QCM-D

results of HAdV-2 adsorption suggest that the RSA model can be applicable to explain the HAdV-2 adsorption.

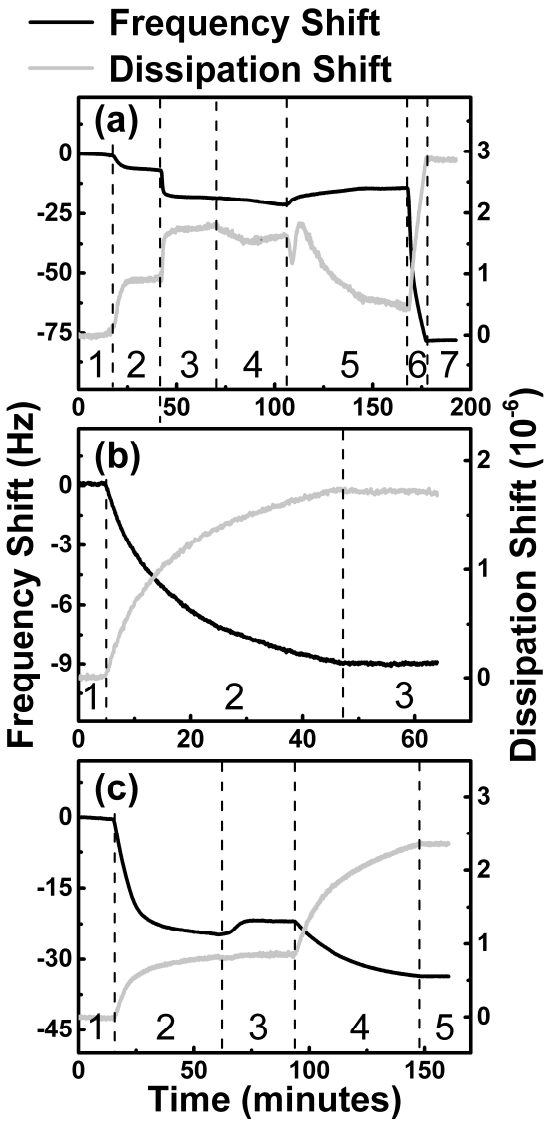

Figure 3.3 The frequency shift $\Delta f_3/3$ (black line and left axis) and the dissipation shift ΔD_3 (grey line and right axis) of HAdV-2 adsorption in the 3 mM $CaCl_2$ solution onto (a) PLL, (b) pristine PVDF and (c) EPS-fouled PVDF. Steps in (a): 1) deionized water; 2) HEPES buffer; 3) 0.1 g/L PLL hydrobromide in the HEPES buffer; 4) HEPES buffer; 5) 3 mM $CaCl_2$ solution; 6) HAdV-2 in the 3 mM $CaCl_2$ solution; 7) 3 mM $CaCl_2$ solution. Steps in (b): 1) 3 mM $CaCl_2$ solution; 2) HAdV-2 in the 3 mM $CaCl_2$ solution; 3) 3 mM $CaCl_2$ solution. Steps in (c): 1) 3 mM $CaCl_2$

solution; 2) EPS in the 3 mM $CaCl_2$ solution; 3) 3 mM $CaCl_2$ solution; 4) HAdV-2 in the 3 mM $CaCl_2$ solution; 5) 3 mM $CaCl_2$ solution.

The RSA model was applied to investigate HAdV-2 adsorption by fitting $\frac{d\Gamma}{dt}$ as a function of Γ with equation 2. In all the $CaCl_2$ solutions, QCM-D data fitting with the RSA model yielded coefficients of determination (R^2) greater than 0.90 on PLL and pristine/EPS-fouled PVDF surfaces, with degrees of freedom higher than 300 for each fitting. The adsorption rate constant k_a, and the area occupied by each adsorbed particle on the surface a, are the two fitting parameters in the RSA model. With the fitted a, the surface coverage (θ) in HAdV-2 adsorption was calculated from the adsorbed mass Γ:

$$\theta = \frac{\Gamma a}{m} \quad (5)$$

The surface coverage θ as a function of time for HAdV-2 adsorption onto the pristine and EPS-fouled PVDF surfaces in different $CaCl_2$ concentrations are shown in Figure 3.4. In all conditions tested, θ increased slower as the adsorption went on, as predicted by the RSA model. We also find that the kinetics of θ depends on the $CaCl_2$ concentration and the surface property. This dependence will be explained by discussing the two fitting parameters, k_a and a, in the following paragraphs.

By definition, the adsorption rate constant k_a is the product of attachment efficiency α and the particle transfer coefficient K, as shown in equation 3. The attachment efficiency α is the ratio of colloids adsorbed to the surface over the number of colloids that collide with the surface, and has been used to investigate the colloid/surface/solvent interaction in porous media [63, 64]. Since all HAdV-2 adsorption experiments were conducted in the same QCM-D chamber with the constant hydrodynamics, the particle transfer coefficient K is a constant. In our adsorption experiment, K is calculated as the slope by fitting k_a as a function of α with equation 3 for both pristine and EPS-fouled PVDF surfaces, as shown in Figure 3.5. The regressions yield R^2 higher than 0.98 with 11 degrees of freedom, indicating a high correlation between k_a and α. The K calculated from HAdV-2 adsorption on the pristine PVDF surface is 0.32 ± 0.01 cm/s, while for the EPS-fouled PVDF, $K = 0.31 \pm 0.01$ cm/s. By performing ANOVA test, we determine that there is no significant difference of K between the pristine and the EPS-fouled PVDF surfaces

(p=0.74). For HAdV-2 adsorption onto the PLL surface, α is assumed to be 1, and $k_a = K = 0.29 \pm 0.02$ cm/s. The constant correlation between k_a and α suggests that the RSA model correctly describes the nature of HAdV-2 adsorption kinetics onto pristine and EPS-fouled PVDF surfaces.

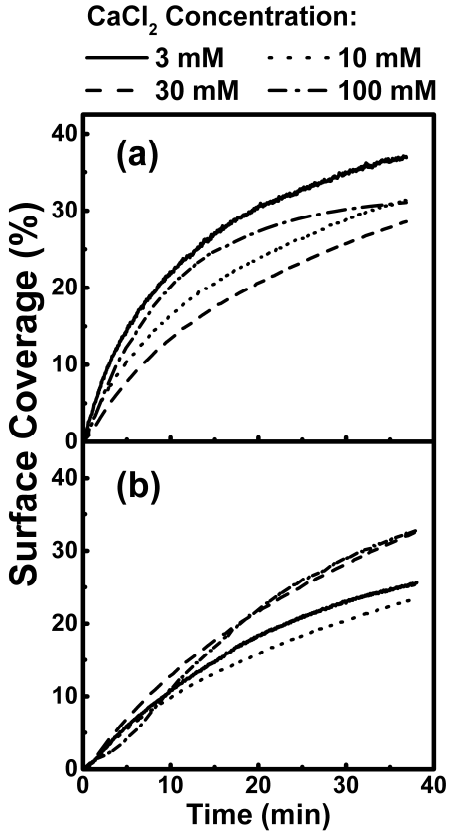

Figure 3.4 The surface coverage θ as a function of time for HAdV-2 adsorption onto (a) pristine PVDF surface and (b) EPS-fouled PVDF surface in 3 mM (solid), 10 mM (dot), 30 mM (dash), and 100 mM (dash dot) $CaCl_2$ solutions.

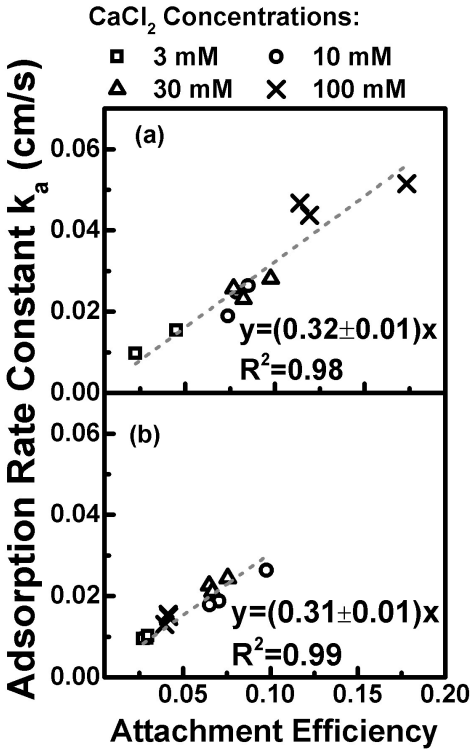

Figure 3.5 The adsorption rate constant k_a as a function of attachment efficiency α on (a) pristine PVDF surface, and (b) EPS-fouled PVDF surface in 3 mM to 100 mM $CaCl_2$ solutions.

The HAdV-2 adsorption rate constant k_a in different $CaCl_2$ concentrations is shown in Figure 3.5. For the pristine PVDF surface, the order of k_a is 3 mM < 10 mM ≈ 30 mM < 100 mM, while for the EPS-fouled PVDF, the order is 3 mM < 100 mM < 10 mM ≈ 30 mM. For the pristine PVDF surface, the trend of k_a agrees with the classic DLVO theory that the increased Ca^{2+} concentration will significantly shield the negative charge of the colloids and the surface [65]. Our previous study of the interaction between MS2 and the PVDF surface has shown that the repulsive force is weakened by calcium cations [10]. For the EPS-fouled PVDF surface, k_a increases as the $CaCl_2$ concentration increases from 3 mM to 10 mM. Ca^{2+} has been reported to be more effective in enhancing virus adsorption onto natural organic matters than monovalent cations like Na^+ and K^+ [66]. Several mechanisms have been proposed to explain the effect of Ca^{2+} enhancing virus adsorption. Classic DLVO theory suggested that the faster adsorption can be attributed to the less negative charge of HAdV-2 in higher $CaCl_2$ concentration. Besides DLVO, it has also been reported that Ca^{2+} could act as a salt bridge between the two negatively

charged surfaces to enhance the adsorption [66, 67]. Another explanation is that Ca^{2+} is an antichaotropic ion increasing the structure of water and thus increasing the hydrophobic interaction between HAdV-2 and PVDF/EPS [14, 15]. In 10 mM and 30 mM $CaCl_2$ solutions on the EPS-fouled PVDF surface, k_a does not significantly change with the $CaCl_2$ concentration. This observation does not agree with the classic DLVO theory. However, similar observations that the adsorption rate does not increase with the cation concentration have been reported for virus and *Cryptosporidium* oocysts [39, 68-70]. The steric interaction between the virus and the surface has been identified as impairing the effect of electrostatic interaction, leading to a stagnation of k_a with the increasing $CaCl_2$ concentration [69]. Compared to the k_a reported in previous QCM-D research [46], the magnitude of k_a in this study is around ten times higher, possibly due to the difference in the flow pattern of QCM-D chambers and in the property of adsorbing particles. In summary, the k_a of HAdV-2 adsorption onto the pristine PVDF surface increases with the $CaCl_2$ concentration, while the steric force between HAdV-2 and EPS inhibits the HAdV-2 adsorption onto the EPS-fouled PVDF surface in $CaCl_2$ concentrations higher than 10 mM.

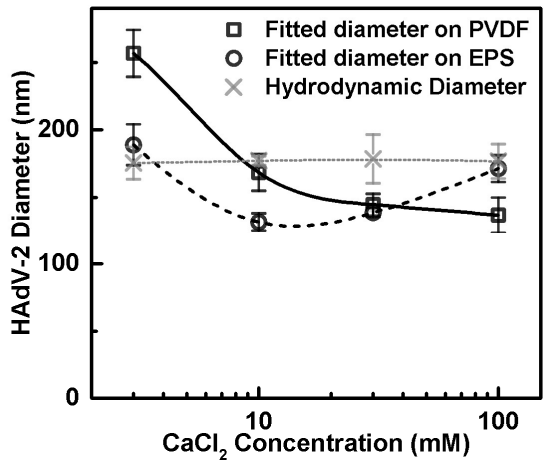

Figure 3.6 The d_{ads} calculated from the fitting parameter a in the RSA model on pristine PVDF surface (square) and EPS-fouled PVDF surface (circle) compared with the hydrodynamic diameters (cross) measured with DLS in $CaCl_2$ solutions from 3 mM to 100 mM.

The other fitting parameter in the RSA model was the area occupied by each adsorbed HAdV-2 particle on the surface a. In order to compare with the hydrodynamic diameter of HAdV-2, a was converted to an equivalent diameter d_{ads}, assuming the area occupied by each HAdV-2 particle was circular. d_{ads} calculated from the RSA model fitting as a function of $CaCl_2$ concentration is shown in Figure 3.6. A discrepancy between d_{ads} and the hydrodynamic diameter of HAdV-2 is found for both the pristine and EPS-fouled PVDF surfaces. The discrepancy can be attributed to the particle-particle and particle-surface interaction forces, which are not considered in the original RSA kinetics model [20, 24]. In the original RSA kinetics model, a successful placement of a particle onto the surface depends on whether the incoming particle overlaps with the previously adsorbed particles. However, surface-particle and particle-particle interactions have been proven to influence whether the placement of an incoming particle would be successful or not [20, 24]. For HAdV-2 adsorption onto the pristine PVDF surface in the 3 mM $CaCl_2$ solution, d_{ads} is larger than the hydrodynamic diameter of HAdV-2 (256 nm vs. 170 nm). The larger d_{ads} may be attributed to the repulsive double layer force between the incoming and adsorbed particles, as previously reported [71]. The effective interaction range of two HAdV-2 particles h^* is defined as:

$$h^* = \frac{d_{ads} - d_v}{2} \quad (6)$$

in which d_v is the diameter of HAdV-2. h^* can be calculated based on d_v and the surface potential of the HAdV-2 (ζ_p) [46, 47, 71]

$$h^* = \frac{1}{2\kappa}\left[\ln\frac{\phi_0}{2\phi_{ch}} - \ln\left(1 + \frac{1}{\kappa d_v}\ln\frac{\phi_0}{2\phi_{ch}}\right)\right] \quad (7)$$

where κ^{-1} is the Debye length, ϕ_0 is the double layer repulsive interaction energy calculated from ζ_p and d_v [72, 73], and ϕ_{ch} is the characteristic energy. Based on equation 7, h^* for HAdV-2 adsorption in the 3 mM $CaCl_2$ solution is 2.6 nm, much smaller than the difference (86 nm) between the hydrodynamic diameter and the d_{ads}. This result indicates that considering only repulsive double layer forces between particles is not sufficient in explaining the HAdV-2 adsorption. The large d_{ads} in the 3mM $CaCl_2$ solution could be attributed to the combination of particle-surface and particle-particle repulsive interaction forces [24].

In $CaCl_2$ concentrations higher than 3 mM, the EPM of HAdV-2 particles became less negative, as shown in Table 3.1, resulting in weaker particle-surface and particle-particle repulsions. For the pristine PVDF surface, the d_{ads} decreases with the $CaCl_2$ concentration. For

the EPS-fouled PVDF surface, a similar decrease of d_{ads} with $CaCl_2$ concentration (3 mM - 30 mM) was observed due to the weakened repulsion. However, with $CaCl_2$ concentration increased from 30 mM to 100 mM, an increase of d_{ads} was observed, and this increase may be due to the steric repulsion between HAdV-2 and the EPS on the surface. The repulsion exerted by EPS at high $CaCl_2$ concentration also influences k_a as shown in Figure 3.5 (b): on the EPS-fouled PVDF surface, k_a in 100 mM $CaCl_2$ was smaller than that in 30 mM $CaCl_2$. It is also noteworthy that in some $CaCl_2$ concentrations, d_{ads} is smaller than the hydrodynamic diameter of HAdV-2. This observation is due to the structure of HAdV-2, which consists of an icosahedron capsid of 90 nm in diameter and 12 protruding fibers of 37 nm in length [52]. A smaller d_{ads} than the hydrodynamic diameter can be attributed to the overlap of fibers for neighboring HAdV-2 on the surface. For the favorable HAdV-2 adsorption onto the positively charged PLL, the attraction between the incoming HAdV-2 and the PLL surface is strong, resulting in the overlapping of the fibers, and the d_{ads} is 103 ± 6 nm for three replicates. In summary, we conclude that repulsive forces towards incoming HAdV-2 particles result in a large area occupied by each HAdV-2 on the surface, while the attractive force between HAdV-2 and the surface leads to the overlapping fibers, which translates into a small area occupied by each adsorbed HAdV-2.

3.5 Conclusion

In recent studies of virus removal by membrane filtration, the significance of virus adsorption onto membranes has been identified [17-19]. However, the influence of virus adsorption on its removal efficiency is not well understood. The knowledge of virus adsorption kinetics and capacity onto membranes is limited. A quantitative understanding of virus adsorption onto membranes can be beneficial for a better control of virus removal by membrane filtration. This knowledge can be also used for developing anti-fouling membranes with high virus removal efficiency.

In this study, we quantitatively determine the HAdV-2 adsorption onto the PVDF surface. The influence of a major membrane foulant, EPS, is also studied to simulate the full scale MBRs. In the QCM-D experiments, we found that the HAdV-2 adsorption onto both the pristine and EPS-fouled PVDF surfaces was irreversible. The HAdV-2 adsorption kinetics and capacity were

interpreted with the random sequential adsorption (RSA) model. In a wide range of $CaCl_2$ concentrations, including the 3mM $CaCl_2$ simulating a municipal wastewater, the RSA model fitting results showed consistent correlations between the adsorption rate constants (k_a) and the attachment efficiencies (α) for both the pristine and EPS-fouled PVDF surfaces. These correlations suggest that the k_a value in the RSA model reflects the interaction forces that dominate the HAdV-2 adsorption onto the surfaces. With the RSA model fitting, we also determined that the $CaCl_2$ concentration and the membrane surface properties influence the HAdV-2 adsorption capacity through particle-particle and particle-surface interactions. If the dominant interaction force was repulsive, the fitted diameter of HAdV-2, d_{ads}, would be larger than the hydrodynamic diameter. If the dominant interaction was attractive, the fibers of adsorbed HAdV-2 particles would overlap, resulting in a d_{ads} smaller than the hydrodynamic diameter. In summary, the RSA model is applicable for describing both the HAdV-2 adsorption kinetics and capacity. Thus, the RSA model can be used to quantitatively evaluate the effect of virus adsorption on its removal efficiency by membrane filtration in future work. The RSA model also has a potential to predict virus transport in other similar environmental systems.

Acknowledgements. This work is supported by the National Science Foundation in CBET Grant 1236672. The authors want to especially acknowledge Bernardo Vazquez Bravo and Aimee Gall for teaching us the techniques to work with human adenovirus. We also want to acknowledge Dean Olson for his help with NMR.

3.6 References

1. Cisneros, B.E.J., B. Jimenez, and T. Asano, *Water reuse: an international survey of current practice, issues and needs*. 2008: IWA Publishing.
2. Toze, S., *Reuse of effluent water—benefits and risks.* Agricultural Water Management, 2006. **80**(1–3): p. 147-159.
3. Fong, T.-T. and E.K. Lipp, *Enteric Viruses of Humans and Animals in Aquatic Environments: Health Risks, Detection, and Potential Water Quality Assessment Tools.* Microbiology and Molecular Biology Reviews, 2005. **69**(2): p. 357-371.

4. Enriquez, C.E., C.J. Hurst, and C.P. Gerba, *Survival of the enteric adenoviruses 40 and 41 in tap, sea, and waste water.* Water Research, 1995. **29**(11): p. 2548-2553.
5. Tanaka, H., et al., *Estimating the safety of wastewater reclamation and reuse using enteric virus monitoring data.* Water Environment Research, 1998. **70**(1): p. 39-51.
6. Kuo, D.H.W., et al., *Assessment of human adenovirus removal in a full-scale membrane bioreactor treating municipal wastewater.* Water Research, 2010. **44**(5): p. 1520-1530.
7. Simmons, F.J., D.H.W. Kuo, and I. Xagoraraki, *Removal of human enteric viruses by a full-scale membrane bioreactor during municipal wastewater processing.* Water Research, 2011. **45**(9): p. 2739-2750.
8. Xagoraraki, I., Z. Yin, and Z. Svambayev, *Fate of Viruses in Water Systems.* Journal of Environmental Engineering, 2014. **140**(7).
9. Shang, C., H.M. Wong, and G.H. Chen, *Bacteriophage MS-2 removal by submerged membrane bioreactor.* Water Research, 2005. **39**(17): p. 4211-4219.
10. Lu, R., D. Mosiman, and T.H. Nguyen, *Mechanisms of MS2 Bacteriophage Removal by Fouled Ultrafiltration Membrane Subjected to Different Cleaning Methods.* Environmental Science & Technology, 2013. **47**(23): p. 13422-13429.
11. Lv, W., et al., *Virus removal performance and mechanism of a submerged membrane bioreactor.* Process Biochemistry, 2006. **41**(2): p. 299-304.
12. Zodrow, K., et al., *Polysulfone ultrafiltration membranes impregnated with silver nanoparticles show improved biofouling resistance and virus removal.* Water Research, 2009. **43**(3): p. 715-723.
13. Farrah, S.R., D.O. Shah, and L.O. Ingram, *Effects of chaotropic and antichaotropic agents on elution of poliovirus adsorbed on membrane filters.* Proceedings of the National Academy of Sciences, 1981. **78**(2): p. 1229-1232.
14. Farrah, S.R., *Chemical factors influencing adsorption of bacteriophage MS2 to membrane filters.* Applied and Environmental Microbiology, 1982. **43**(3): p. 659-663.
15. Shields, P.A. and S.R. Farrah, *Influence of salts on electrostatic interactions between poliovirus and membrane filters.* Applied and Environmental Microbiology, 1983. **45**(2): p. 526-531.
16. Lukasik, J., et al., *Influence of salts on virus adsorption to microporous filters.* Applied and Environmental Microbiology, 2000. **66**(7): p. 2914-2920.

17. Jackson, N.B., et al., *Internal virus polarization model for virus retention by the Ultipor® VF Grade DV20 membrane.* Biotechnology Progress, 2014. **30**(4): p. 856-863.
18. Lute, S., et al., *Phage passage after extended processing in small-virus-retentive filters.* Biotechnology and Applied Biochemistry, 2007. **47**(3): p. 141-151.
19. Lu, R., et al., *Effect of virus influent concentration on its removal by microfiltration: The case of human adenovirus 2.* Journal of Membrane Science, 2016. **497**: p. 120-127.
20. Adamczyk, Z., et al., *Structure and ordering in localized adsorption of particles.* Journal of Colloid and Interface Science, 1990. **140**(1): p. 123-137.
21. Adamczyk, Z., B. Siwek, and M. Zembala, *Kinetics of localized adsorption of particles on homogeneous surfaces.* Journal of Colloid and Interface Science, 1992. **151**(2): p. 351-369.
22. Adamczyk, Z., B. Siwek, and M. Zembala, *Reversible and irreversible adsorption of particles on homogeneous surfaces.* Colloids and Surfaces, 1992. **62**(1–2): p. 119-130.
23. Adamczyk, Z., et al., *Kinetics of localized adsorption of colloid particles.* Advances in Colloid and Interface Science, 1994. **48**: p. 151-280.
24. Oberholzer, M.R., et al., *2-D and 3-D Interactions in Random Sequential Adsorption of Charged Particles.* Journal of Colloid and Interface Science, 1997. **194**(1): p. 138-153.
25. Hemmersam, A.G., et al., *Fibronectin adsorption on gold, Ti-, and Ta-oxide investigated by QCM-D and RSA modelling.* Journal of Colloid and Interface Science, 2008. **320**(1): p. 110-116.
26. Johnson, P.R. and M. Elimelech, *Dynamics of colloid deposition in porous media: Blocking based on random sequential adsorption.* Langmuir, 1995. **11**(3): p. 801-812.
27. Fong, T.-T., et al., *Quantitative Detection of Human Adenoviruses in Wastewater and Combined Sewer Overflows Influencing a Michigan River.* Applied and Environmental Microbiology, 2010. **76**(3): p. 715-723.
28. Pina, S., et al., *Viral Pollution in the Environment and in Shellfish: Human Adenovirus Detection by PCR as an Index of Human Viruses.* Applied and Environmental Microbiology, 1998. **64**(9): p. 3376-3382.
29. Uhnoo, I., et al., *Importance of enteric adenoviruses 40 and 41 in acute gastroenteritis in infants and young children.* Journal of Clinical Microbiology, 1984. **20**(3): p. 365-372.

30. Wang, D., K. Li, and W. Teo, *Preparation and characterization of polyvinylidene fluoride (PVDF) hollow fiber membranes.* Journal of Membrane Science, 1999. **163**(2): p. 211-220.
31. Wang, P., et al., *Plasma-induced immobilization of poly(ethylene glycol) onto poly(vinylidene fluoride) microporous membrane.* Journal of Membrane Science, 2002. **195**(1): p. 103-114.
32. Chang, I.-S. and C.-H. Lee, *Membrane filtration characteristics in membrane-coupled activated sludge system — the effect of physiological states of activated sludge on membrane fouling.* Desalination, 1998. **120**(3): p. 221-233.
33. Cho, B. and A. Fane, *Fouling transients in nominally sub-critical flux operation of a membrane bioreactor.* Journal of Membrane Science, 2002. **209**(2): p. 391-403.
34. Le-Clech, P., V. Chen, and T.A.G. Fane, *Fouling in membrane bioreactors used in wastewater treatment.* Journal of Membrane Science, 2006. **284**(1-2): p. 17-53.
35. Sirikanchana, K., J.L. Shisler, and B.J. Mariñas, *Effect of exposure to UV-C irradiation and monochloramine on adenovirus serotype 2 early protein expression and DNA replication.* Applied and Environmental Microbiology, 2008. **74**(12): p. 3774-3782.
36. Liu, H. and H.H.P. Fang, *Extraction of extracellular polymeric substances (EPS) of sludges.* Journal of Biotechnology, 2002. **95**(3): p. 249-256.
37. Ohshima, H., *Electrophoretic Mobility of Soft Particles.* Journal of Colloid and Interface Science, 1994. **163**(2): p. 474-483.
38. Ohshima, H., *Electrostatic interaction of soft particles.* Advances in Colloid and Interface Science.
39. Liu, Y., et al., *Deposition of Cryptosporidium parvum Oocysts on Natural Organic Matter Surfaces: Microscopic Evidence for Secondary Minimum Deposition in a Radial Stagnation Point Flow Cell.* Langmuir, 2009. **25**(3): p. 1594-1605.
40. Herzberg, M.H.M., et al., *Surface Properties and Reduced Biofouling of Graft-Copolymers That Possess Oppositely Charged Groups.* Biomacromolecules, 2011. **12**(4): p. 1169-1177.
41. Sweity, A., et al., *pH effects on the adherence and fouling propensity of extracellular polymeric substances in a membrane bioreactor.* Journal of Membrane Science, 2011. **378**(1-2): p. 186-193.

42. Nguyen, T.H. and M. Elimelech, *Adsorption of Plasmid DNA to a Natural Organic Matter-Coated Silica Surface: Kinetics, Conformation, and Reversibility.* Langmuir, 2007. **23**(6): p. 3273-3279.
43. Chen, K.L. and M. Elimelech, *Aggregation and deposition kinetics of fullerene (C-60) nanoparticles.* Langmuir, 2006. **22**(26): p. 10994-11001.
44. Nguyen, T.H. and M. Elimelech, *Plasmid DNA adsorption on silica: Kinetics and conformational changes in monovalent and divalent salts.* Biomacromolecules, 2007. **8**(1): p. 24-32.
45. Schaaf, P. and J. Talbot, *Surface exclusion effects in adsorption processes.* The Journal of Chemical Physics, 1989. **91**(7): p. 4401-4409.
46. Kubiak, K., Z. Adamczyk, and M. Oćwieja, *Kinetics of Silver Nanoparticle Deposition at PAH Monolayers: Reference QCM Results.* Langmuir, 2015. **31**(10): p. 2988-2996.
47. Adamczyk, Z., et al., *Streaming potential studies of colloid, polyelectrolyte and protein deposition.* Advances in Colloid and Interface Science, 2010. **153**(1–2): p. 1-29.
48. Van Oostrum, J. and R.M. Burnett, *Molecular composition of the adenovirus type 2 virion.* Journal of Virology, 1985. **56**(2): p. 439-448.
49. Schaaf, P. and J. Talbot, *Kinetics of random sequential adsorption.* Physical review letters, 1989. **62**(2): p. 175.
50. Sauerbrey, G., *Verwendung von Schwingquarzen zur Wägung dünner Schichten und zur Mikrowägung.* Zeitschrift für physik, 1959. **155**(2): p. 206-222.
51. Horwitz, M.S., *Adenoviruses.* Fields virology, 2001. **2**: p. 2301-2326.
52. Devaux, C., et al., *Structure of adenovirus fibre: I. Analysis of crystals of fibre from adenovirus serotypes 2 and 5 by electron microscopy and X-ray crystallography.* Journal of Molecular Biology, 1990. **215**(4): p. 567-588.
53. Trilisky, E.I. and A.M. Lenhoff, *Sorption processes in ion-exchange chromatography of viruses.* Journal of Chromatography A, 2007. **1142**(1): p. 2-12.
54. De Gusseme, B., et al., *Virus disinfection in water by biogenic silver immobilized in polyvinylidene fluoride membranes.* Water Research, 2011. **45**(4): p. 1856-1864.
55. Düputell, D. and E. Staude, *Heterogeneous modification of ultrafiltration membranes made from poly(vinylidene fluoride) and their characterization.* Journal of Membrane Science, 1993. **78**(1–2): p. 45-51.

56. Han, M.J., G.N.B. Baroña, and B. Jung, *Effect of surface charge on hydrophilically modified poly(vinylidene fluoride) membrane for microfiltration.* Desalination, 2011. **270**(1–3): p. 76-83.
57. Wilson, M.A., *APPLICATIONS OF NUCLEAR MAGNETIC RESONANCE SPECTROSCOPY TO THE STUDY OF THE STRUCTURE OF SOIL ORGANIC MATTER.* Journal of Soil Science, 1981. **32**(2): p. 167-186.
58. Ma, H., H.E. Allen, and Y. Yin, *Characterization of isolated fractions of dissolved organic matter from natural waters and a wastewater effluent.* Water Research, 2001. **35**(4): p. 985-996.
59. Thorn, K.A., D.W. Folan, and P. MacCarthy, *Characterization of the International Humic Substances Society standard and reference fulvic and humic acids by solution state carbon-13 (13C) and hydrogen-1 (1H) nuclear magnetic resonance spectrometry*. 1991: US Department of the Interior, US Geological Survey.
60. Averett, R.C., et al., *Humic substances in the Suwannee River, Georgia; interactions, properties, and proposed structures*. 1994, USGPO; US Geological Survey, Map Distribution.
61. Stevenson, F.J., *Humus chemistry, genesis, composition, reactions*. Humus chemistry, genesis, composition, reactions. 1982. 443.
62. Dixon, M.C., *Quartz Crystal Microbalance with Dissipation Monitoring: Enabling Real-Time Characterization of Biological Materials and Their Interactions.* Journal of Biomolecular Techniques : JBT, 2008. **19**(3): p. 151-158.
63. Elimelech, M. and C.R. O'Melia, *Kinetics of deposition of colloidal particles in porous media.* Environmental Science & Technology, 1990. **24**(10): p. 1528-1536.
64. Cail, T.L. and M.F. Hochella Jr, *The effects of solution chemistry on the sticking efficiencies of viable Enterococcus faecalis: An atomic force microscopy and modeling study.* Geochimica et Cosmochimica Acta, 2005. **69**(12): p. 2959-2969.
65. Overbeek, J.T.G., *The rule of Schulze and Hardy.* Pure and Applied Chemistry, 1980. **52**(5): p. 1151-1161.
66. Pham, M., E.A. Mintz, and T.H. Nguyen, *Deposition kinetics of bacteriophage MS2 to natural organic matter: Role of divalent cations.* Journal of Colloid and Interface Science, 2009. **338**(1): p. 1-9.

67. Kessick, M. and R. Wagner, *Electrophoretic mobilities of virus adsorbing filter materials.* Water Research, 1978. **12**(4): p. 263-268.
68. Kuznar, Z.A. and M. Elimelech, *Role of surface proteins in the deposition kinetics of Cryptosporidium parvum oocysts.* Langmuir, 2005. **21**(2): p. 710-716.
69. Yuan, B.L., M. Pham, and T.H. Nguyen, *Deposition Kinetics of Bacteriophage MS2 on a Silica Surface Coated with Natural Organic Matter in a Radial Stagnation Point Flow Cell.* Environmental Science & Technology, 2008. **42**(20): p. 7628-7633.
70. Janjaroen, D., et al., *Role of Divalent Cations on Deposition of Cryptosporidium parvum Oocysts on Natural Organic Matter Surfaces.* Environmental Science & Technology, 2010. **44**(12): p. 4519-4524.
71. Adamczyk, Z., *Particles at interfaces: interactions, deposition, structure*. Vol. 9. 2006: Academic Press.
72. Hlavacek, M. and J. Remy, *Simple relationships among zeta potential, particle size distribution, and cake specific resistance for colloid suspensions coagulated with ferric chloride.* Separation science and technology, 1995. **30**(4): p. 549-563.
73. Gregory, J. and C.R. O'Melia, *Fundamentals of flocculation.* Critical Reviews in Environmental Science and Technology, 1989. **19**(3): p. 185-230.

CHAPTER 4

MODIFYING ULTRAFILTRATION MEMBRANES WITH GRAFTED ZWITTERIONIC POLYMER HYDROGELS FOR IMPROVED VIRUS REMOVAL

Submit to *Water Research*, 2016

Ruiqing Lu, Chang Zhang, Maria Piatkovsky, Mathias Ulbricht, Moshe Herzberg, Thanh H. Nguyen. Modifying ultrafiltration membranes with grafted zwitterionic polymer hydrogels for improved virus removal

4.1 Abstract

Potable water reuse has been adopted by cities suffering water scarcity in recent years. The microbial safety in water reuse, especially with respect to pathogenic viruses, is still a concern for water consumers. Membrane filtration can achieve sufficient removal of pathogenic viruses without disinfection byproducts, but the required energy is intensive. In this study, we graft-polymerize zwitterionic SPP ([3-(methacryloylamino) propyl] dimethyl (3-sulfopropyl) ammonium hydroxide) from a 150 kDa ultrafiltration polyethersulfone membrane to achieve a significantly higher virus removal. The redox-initiated graft-polymerization was performed in an aqueous solution during filtration of the monomer and initiators, allowing for functionalizing the membrane pores with hydrophilic polySPP. Bacteriophage MS2 and human adenovirus type 2 (HAdV-2) were used as surrogates for pathogenic human norovirus and human adenovirus. The grafting resulted in ~ 18 % loss of the membrane permeability but an increase of 4 $\log_{10}$ in HAdV-2 removal and 3 $\log_{10}$ in MS2 removal. The pristine and the grafted membranes were both conditioned with soluble microbial products (SMP) extracted from a full-scale membrane bioreactor (MBR) in order to test the virus removal after fouling the membranes. After fouling, the HAdV-2 removal by the grafted membrane was 1 $\log_{10}$ higher than that of the pristine membrane. For MS2, the grafted membrane after fouling with SMP achieved an additional 5

$\log_{10}$ removal compared to the unmodified membrane. The simple graft-polymerization functionalization of commercialized membrane achieving enhanced virus removal efficiency highlights the promise of membrane filtration for pathogen control in potable water reuse.

4.2 Introduction

Direct potable water reuse facilities, which use treated municipal wastewater as the source for their water supply without any environmental buffer, have recently been in practice to overcome the water scarcity in Big Spring and Wichita Falls, Texas [1]. Microbial safety is a lasting concern in water reuse [2], and this concern needs to be further considered in the context of direct potable reuse. In raw sewage, the concentration of pathogenic virus can be up to 10^7 virus/L [3, 4]. Among all waterborne pathogens, viruses have the smallest size and therefore are the hardest to be removed by sedimentation and filtration [5]. Though disinfection has been adopted for pathogen removal, neither UV nor chlorine achieved satisfactory virus removal in wastewater treatment [6]. This observed insufficient virus removal could pose a threat to public health [7]. For example, human norovirus was estimated to be the second leading infectious cause in gastroenteritis-associated mortality [8]. Human adenovirus can cause multiple diseases and is even fatal for immune-compromised water users [9]. Insufficient removal of human adenovirus in municipal wastewater has been detected to contaminate drinking water sources, including the Great Lakes [10]. The necessity to improve virus removal in potable reuse is urgent to ensure public safety.

Virus removal in water reuse should not solely rely on disinfection. In full-scale wastewater treatment plants, the contribution of secondary treatments on virus removal is much larger than that of disinfection, probably due to the high concentration of nutrients in wastewater increasing the consumption of disinfectants [6]. The membrane bioreactor (MBR) showed its promise to achieve high virus removal [3]. Although up to 6 $\log_{10}$ virus removal could be achieved by the MBR with fouled membranes, [11-14], significantly decreased membrane permeability was also observed. Thus, high virus removal in the MBR occurs with increased operation costs.

The improved virus removal by foulants was firstly attributed to the membrane pore plugging and pore restriction [11, 15]. Recent research found that the increased virus removal was

accomplished by both the decrease of pore size and the increasing repulsive forces exerted by foulants [16]. Other mechanistic studies suggest that the virus-membrane interaction forces are significant in determining the virus removal efficacy in membrane filtration [14]. The repulsive virus-membrane interaction forces prevent virus entering the membrane pores even in the case that the pore size was larger than the size of the virus [17]. By tuning the virus-membrane interaction forces through pH, ionic strength, and ion types, changes in virus removal were observed [18, 19]. Besides the virus-membrane interaction forces, virus transport through the membrane is also influenced by the hydrodynamic forces. The water flow near the membrane surface has the effect of sucking the viral particles towards the membrane [20]. Due to the slow diffusion of viruses compared to the convective forces acting on the virions, the viruses rejected by the membrane accumulate on the membrane surface, leading to an increase of the local concentration of viruses. As a result, the virus concentration in the permeate also increases. This mechanism in virus removal was indirectly proved by investigating the virus removal dynamics [20, 21], and directly observed with confocal microscopy [18, 22, 23]. Based on previous knowledge, we hypothesize that the virus removal by membrane filtration can be improved by inducing repulsive virus-membrane interaction forces to prevent virus approaching the membrane surface.

In this study, we aim to graft hydrogels on a conventional ultrafiltration membrane as a barrier for virus accumulation on the membrane surface. Since hydrogel may have a minor influence on the water flux through the membrane, the virus removal would be improved without sacrificing the membrane permeability. Membrane modification using grafted hydrogels was shown in various applications to prevent the attachment of macromolecules, bacteria, and microbial biofilms based on chemical ("low-fouling" monomers) and physical (dilution) principles [24]. The latter effect is due to the high water content of the hydrogel layer. At the same time, the polymeric hydrogel network can prevent particles from coming in direct contact with the solid membrane surface. The use of hydrogel grafted layers on ultrafiltration membranes for improved virus rejection could be an attractive option due to their low hydraulic resistance and their minimum impact on membrane permeability. Such virus-membrane repulsion forces are introduced by grafting zwitterionic hydrogel polymers onto a commercially available ultrafiltration membrane using a previously developed method [25, 26]. Since membrane fouling usually takes place during wastewater filtration and the virus removal process, we also studied

the virus removal with the membrane fouled by soluble microbial products (SMP) extracted from the biomass of a full-scale MBR. To examine the removal for viruses of different sizes, the membrane was challenged with a small virus, bacteriophage MS2 (~30 nm) [16], and a large virus, human adenovirus 2 (HAdV-2) (~170 nm) [21]. MS2 is a surrogate for the pathogenic human norovirus for their similarity in size and structure [27]. The results of this study further illustrate the mechanism of virus removal in ultrafiltration, and more importantly, can provide an alternative in membrane development targeting better virus control in water reuse.

4.3 Methods

UF membrane and redox-initiated grafting of zwitterionic hydrogel layer. A commercially available ultrafiltration membrane (NADIR® PM UP 150) was graft-polymerized with a hydrogel coating of SPP ([3-(methacryloylamino) propyl] dimethyl (3-sulfopropyl) ammonium hydroxide). The membrane sheets were received from MICRODYN NADIR GmbH (Wiesbad, Germany). The nominal molecular weight cutoff (MWCO) of this polyethersulfone (PES) membrane is 150 kDa. Redox-initiated graft-polymerization was performed in an aqueous solution at room temperature, based on our previously published procedure [28, 29]. SPP (Sigma-Aldrich, Israel) was graft-polymerized at a concentration of 0.5 M, and the initiators (Sigma-Aldrich, Israel) were potassium persulfate ($K_2S_2O_8$, 0.01 M) and potassium metabisulfite ($K_2S_2O_5$, 0.01 M). Both SPP monomer and the two initiators were dissolved in double distilled water and immediately filtered through the UF membrane at a constant pressure of 0.15±0.02 bar. Filtration was conducted using an Amicon 8050 stirred cell (Millipore Co.) continuously fed with the SPP and the initiators solution with a peristaltic pump, similar to the system used for virus filtration and conditioning with SMP material (Figure 4.1). Membrane permeability analysis of the pristine and modified membranes was conducted with deionized water under the pressure ranging from 0.28 to 0.69 bar.

ATR-FTIR analysis of the grafted and pristine membranes. Attenuated total reflection Fourier transform infra-red (ATR-FTIR) spectroscopy measurements of both sides of the membrane were recorded on a VERTEX 70/80 standard system spectrophotometer, using a germanium crystal (BRUKER Optiks, Ettlingen, Germany). The membranes were completely dried overnight under vacuum at 25 ºC, prior to the measurement.

Contact angle measurements. The static contact angle for the captive air bubble was conducted on the modified and pristine membranes using an OCA-20 contact angle analyzer by DataPhysics Instruments (Filderstadt, Germany). Membrane pieces were submerged in deionized water (pH=6.2), 10 mM NaCl (pH=6.2), and 3 mM $CaCl_2$ solution (pH=8.0), which was adjusted with $NaHCO_3$ and allowed to equilibrate for at least one hour. A 5 µl bubble was then deposited on the surface from below and imaged using a camera. A surface baseline was then drawn right above the bubble profile, and the angle at the line of 3-phase contact was calculated.

Propagation, purification, and quantification of viruses. Bacteriophage MS2 (ATCC 15597-B1) and HAdV-2 (ATCC VR-846) were supplied by American Type Culture Collection. Details of virus propagation and purification were published previously [16, 21]. Briefly, MS2 was propagated with *Escherichia coli* (ATCC 15597) in the tryptic soy broth liquid media. A 10 kDa MWCO membrane (Koch Membranes, United States) was applied to retain the MS2 virus and wash off media residue. The MS2 stock was further purified with 10% PEG 6000. The MS2 concentration was determined with the plaque-forming unit (PFU) assay. HAdV-2 was propagated with the A549 human lung carcinoma cells supplied by Diagnostic Hybrids. The media for HAdV-2 propagation was Ham's F12K supplemented with fetal bovine serum, penicillin, streptomycin, and amphotericin B. After propagation, large cellular debris were removed with a 0.45 µm membrane (Corning). The media residue was washed with 1 mM

$NaHCO_3$ solution, and the HAdV-2 was retained with a 100 kDa MWCO membrane (Koch Membranes, United States). The concentration of HAdV-2 was quantified with real-time PCR, as previously reported [21, 30]. The hydrodynamic diameters of purified MS2 and HAdV-2 were determined by dynamic light scattering with a Zetasizer (Malvern, UK) in a 3 mM $CaCl_2$ solution at pH=8.0 buffered with $NaHCO_3$.

Soluble microbial products extracted from a full-scale MBR. Soluble microbial products (SMP) were extracted from the biomass sampled from a full-scale MBR in the Traverse City Wastewater Treatment Plant (Traverse City, Michigan, United States) following a previously reported method [16]. Briefly, the biomass was centrifuged at 5,000 rpm for 15 minutes for precipitation. The supernatant was filtered with a 0.22 μm membrane (Millipore, Germany). Ions in the extracted SMP were removed by dialysis versus deionized water with a 3,500 Da dialysis membrane (ThermoFisher, United States). The concentration of the SMP after dialysis was determined in terms of total organic carbon (TOC=19.5 mg/L) (Shimadzu, Japan). Fractions of the extracted SMP were characterized with a liquid chromatography with organic carbon detection (LC-OCD) (DOC-LABOR Model 8, Germany) [31]. 1 mL of the extracted SMP was used for the LC-OCD analysis, and the analysis time was set at 130 minutes [32]. Organic matters in the SMP were fractionized into biopolymers, humic substances, building blocks, low molecular weight neutrals, and low molecular weight acids based on the retention time [31]. The concentration of each fraction was calculated with the ChromCALC® software by integrating the area of each peak. Before dialysis, the cations in the SMP were determined with an ICP-MS (Perkin-Elmer, United States). The dominant cations were Ca^{2+} and Mg^{2+} with a total concentration of 3.40±0.01 mM, and the pH was 8.0. Therefore, 3 mM $CaCl_2$ with pH adjusted to 8.0 by $NaHCO_3$ was set as the ionic condition for the filtration experiment.

Virus removal by the graft polymerized and the pristine membranes. A bench-scale flat sheet membrane filtration unit was built for the virus filtration experiments with the schematic diagram shown in Figure 4.1. Filtration was operated in the dead-end mode with a constant pressure of 0.69 bar. The pressure during the filtration was monitored with a pressure gauge, and the flow rate of the pump (Masterflex, United States) was manually adjusted to keep the pressure constant. The permeate flow rate during filtration was recorded with an electronic balance (Ohaus, United States) connected to a computer. Before virus filtration experiments, the permeate flux of the membrane was measured with deionized (DI) water for at least 1 hour.

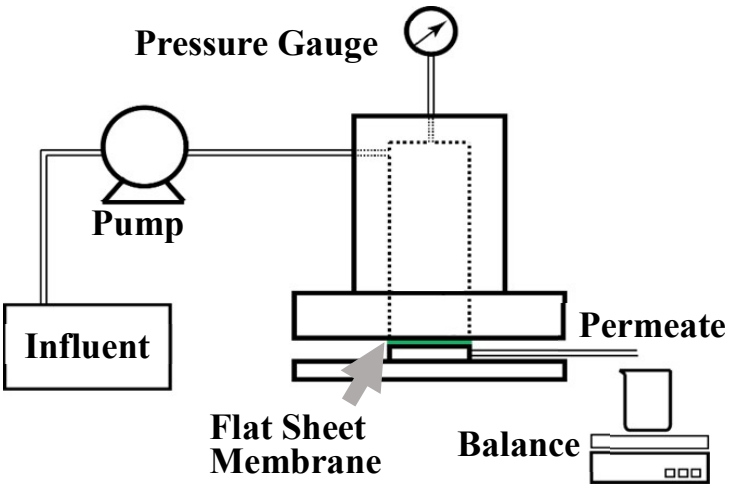

Figure 4.1 The schematic diagram of the bench scale filtration unit for virus removal by flat sheet ultrafiltration membranes.

MS2 and HAdV-2 were separately filtered with the modified and the unmodified membranes. The virus influent solution was prepared by diluting the virus stock solution with 3 mM $CaCl_2$ solution at pH=8.0, which was adjusted with $NaHCO_3$. The influent concentration of MS2 was 2.3×10^9 PFU/mL, and for HAdV-2 it was 3.0×10^9 virus/mL. For each filtration

experiment, the virus concentration of influent solutions ($C_{influent}$) and permeate samples ($C_{permeate}$) were determined. Permeate samples were collected intermittently during the filtration experiment. The values of virus removal in $\log_{10}$ were calculated with the equation below:

$$\text{Virus removal } (log_{10}) = -log_{10}\frac{C_{permeate}}{C_{influent}} \quad (1)$$

The virus removal was also determined with membranes fouled with SMP. The SMP at a concentration of 19.5 mg TOC/L in 3 mM $CaCl_2$ (pH=8.0) was filtered through the modified and the unmodified membranes at a constant pressure of 0.69 bar until the volume of the permeate reached 25 mL. The permeate of the SMP solution was collected and the concentration was determined in TOC. The SMP removal efficacy by the unmodified and the modified membranes were $12 \pm 0.3\%$ and $19 \pm 2\%$, respectively. After SMP fouling, the feed solution was changed to the virus solution and the virus filtration was conducted in the same way as that for the membranes without foulants, to determine the virus removal efficiency by the membranes with SMP foulants.

Interaction forces on membrane surface measured by the atomic force microscope (AFM). An Asylum MFP-3D AFM (Santa Barbara, CA, USA) was applied to measure the interaction forces between a sphere silica probe with a 5 μm diameter (Novascan, United States) and the unmodified/modified membranes in 1-100 mM NaCl and 3 mM $CaCl_2$ solutions at pH=8.0 buffered with $NaHCO_3$. The nominal spring constant of the cantilever was 0.06 N/m, and the actual spring constant was determined with a freshly cut mica disk in the air. In contact mode, force curves were taken on 5 randomly selected locations on each membrane surface. To minimize inherent variability, more than 10 force curves were taken at each location. Only

repulsive forces were observed when the probe approached the membrane surface. The decay length (κ^{-1}) of the approaching force curves was determined by fitting the repulsive force F as a function of the separation distance D with the equation below, in which B is a pre-exponential constant [33, 34].

$$F = B \times \exp(-\kappa D) \quad (2)$$

4.4 Results

ATR-FTIR characterization. ATR-FTIR spectra were taken on both sides of the modified membranes to validate the grafting success. Compared to the spectrum of the unmodified membrane, the modified membrane spectrum has three additional peaks, corresponding to the grafted polySPP functional groups (Figure 4.2 (a)). These peaks are 1663 cm^{-1}, 1038 cm^{-1}, and 928 cm^{-1}, corresponding to the stretching of the C=O bond of secondary amide group, the presence of the sulfonic groups, and the presence of quaternary amines, respectively. The support side is a certain polyolefine, non-disclosed by the membrane manufacturer, and the corresponding FTIR spectrum was detected. Analysis of the support layer (Figure 4.2 (b)) revealed two additional peaks at 1038 cm^{-1} and 928 cm^{-1} for the modified membrane, indicating the presence of sulfonic groups and quaternary amine, respectively. These results show successful modification of the membrane on the inlet side by redox-polymerization. The presence of the two out of three additional peaks on the outlet side is another indication for the successful modification of the membrane pores with polySPP, since the penetration depth of the FTIR beam is lower than 3 µm. Therefore, the observed spectrum taken at the outlet side of the membrane cannot be influenced from the modification on the inlet side of the membrane. Indeed, the significant increase of hydrophilicity for both the inlet side and the outlet side of the membrane is validated in the contact angle results (Table 4.1), which also suggests that the polySPP grafted within the membrane pores.

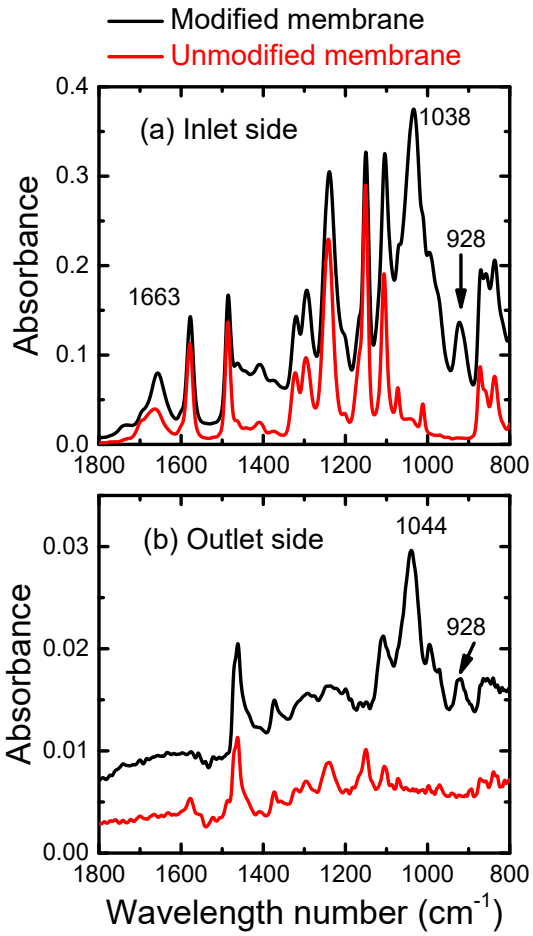

Figure 4.2 ATR-FTIR spectra of the pristine (red) and SPP-modified (black) PES membranes taken at their active-feed (a) and support-permeate (b) sides.

Contact angles of the modified and pristine membranes' surfaces were measured to assess the changes in the membranes' hydrophilicities caused by the modification. At least 3 measurements were done for each surface type, and the results are summarized in Table 4.1. In both 10 mM NaCl and 3 mM $CaCl_2$ solutions, the modification increased the hydrophilicity of PES. Notably, in the presence of deionized water, almost no change in the contact angle measurement was detected, likely due to the collapse of the polySPP hydrogel in the presence of deionized water, as also shown in previous studies [24, 25]. Membrane permeability to deionized water was tested before and after grafting under the pressure ranging from 0.28 to 0.69 bar: the initial permeability of the pristine membrane was 21.6±0.8 $\frac{\mathrm{L}}{m^2\,h}$/Bar (LMH/Bar) and the permeability

after membrane graft-polymerization was 17.7±0.6 LMH/Bar. The decrease in membrane permeability was 18±3%.

Table 4.1 Contact angles of the pristine and the modified PES membranes measured by the air captive bubble method.

	Liquid	Contact angle (PES pristine)	Contact angle (PES modified using 0.5M SPP solution)
Feed side	Deionized water	49.9±2.6	51.0±2.7
	10 mM NaCl solution	46.4±2.2	21.2±4.2
	3 mM $CaCl_2$ solution	48.1±5.7	36.3±2.2
Outlet side	Deionized water	58.9±4.2	58.4±3.8
	10 mM NaCl solution	53.9±0.9	50.7±1.8
	3 mM $CaCl_2$ solution	61.8±1.7	45.6±2.9

AFM force measurement on membranes. The representative AFM approaching force curves on unmodified and modified membrane surfaces are shown in Figure 4.3. In 1 to 100 mM NaCl solutions and 3 mM $CaCl_2$ solution, the force curves on the unmodified membrane are similar to that on the mica surface, which was used as a reference surface for the electrostatic interaction. The range of repulsive interactions decreased with the ionic strength for mica and the unmodified membrane. Fitting the force curves with Equation 2, the decay length on the unmodified membrane in 1 mM, 10 mM, 100 mM NaCl, and 3 mM $CaCl_2$ are 9.1±0.6 nm, 3.5±0.4 nm, 1.1±0.3 nm, and 3.1±0.4 nm, respectively. On the mica surface they are 9.4±0.8 nm, 3.4±0.5 nm, 1.1±0.4 nm, and 3.1±0.4 nm, respectively. The measured decay lengths on both the mica surface and the unmodified membrane agree with the calculated Debye lengths for different ionic strengths, suggesting the dominant role of the electrostatic interaction force between the AFM probe and the unmodified membrane surface.

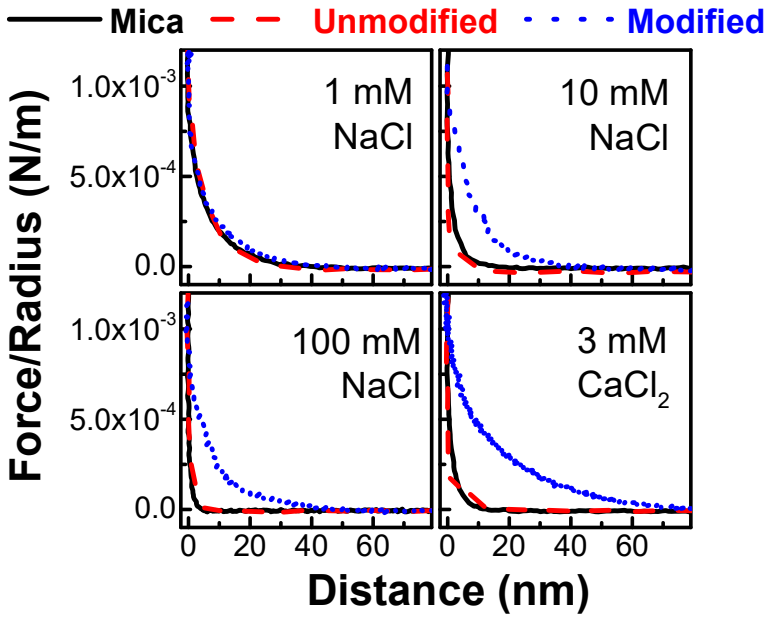

Figure 4.3 Representative approaching force curve on mica (black line), the modified (blue dots) and the unmodified (red dash) membranes in different ionic conditions.

The modified membrane surface differed from the reference surface in the repulsion range. The repulsion range on the modified membrane surface did not decrease with the ionic strength. For ionic strength larger than 1 mM, the repulsion range and the magnitude of the repulsion force on the modified membrane was much larger than that on the unmodified membrane. The longer interaction range and the stronger repulsion forces observed for the modified membrane infer that the SPP gel layer served as a barrier for particles approaching the solid PES surface of the modified membrane.

Characterization of the SMP foulant with LC-OCD. The components in the extracted SMP were characterized with LC-OCD. The relative signal response for organic carbon detection (OCD), UV detection at 254 nm (UVD), and organic nitrogen detection (OND) are shown as functions of retention time in Figure 4.4. The peak at the retention time of 33 minutes for OCD and OND indicates high molecular weight biopolymers, and the minor peak for UVD suggests that there are low contents of unsaturated bonds [31]. By integrating the peak area, the biopolymers account for 30.8% of the dissolved organic carbon in the SMP. The major compositions of biopolymers are proteins and polysaccharides [35]. By analyzing the OND

signal, the percentage of protein in biopolymers was 48%. With the peak eluted at 44 minutes, humic substances were detected [31]. The fraction of humic substances in the SMP is 56.4%, and the content of unsaturated bonds is high in humic substances, as detected in UVD. Concentrations of low molecular weight compounds are low in the extracted SMP.

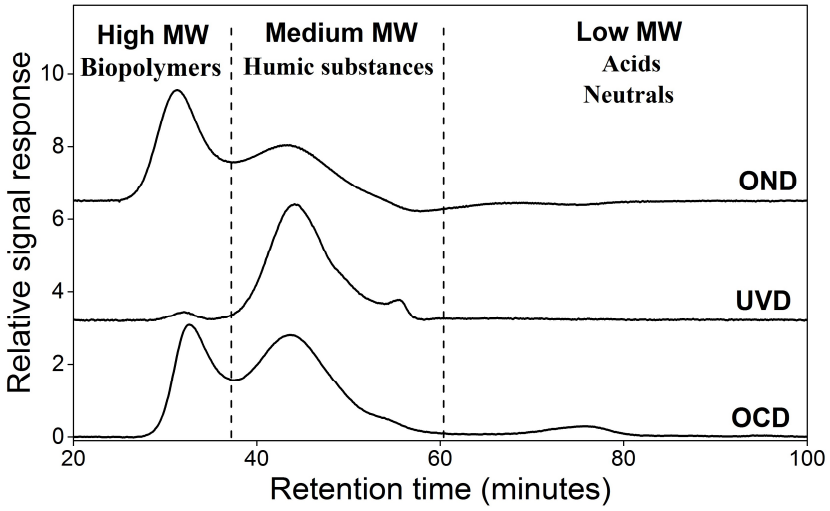

Figure 4.4 LC-OCD chromatogram of the SMP extracted from the full-scale MBR biomass with relative response signal for organic carbon detection (OCD), UV detection at 254 nm (UVD), and organic nitrogen detection (OND).

MS2 and HAdV-2 filtration by clean unmodified and modified membranes: virus removal and the change of permeate flux during filtration. The HAdV-2 removal by the modified and the unmodified membranes as a function of the filtration time is shown in the scatters plots on Figure 4.5 (a). With the unmodified membrane, the HAdV-2 removal was between 2 to 3 $\log_{10}$, and the removal efficiency increased with the filtration time. For all effluent samples collected with the modified membrane, the HAdV-2 removal was higher than 6 $\log_{10}$. The permeate flux of the modified membrane was 18% lower than that of the unmodified membrane at the beginning of the filtration as expected, since an average decrease of membrane permeability was18±3%, as determined above (cf. section 3.1). After filtering 6 mL of HAdV-2 influent at initial permeate flux of 14.7 LMH, the permeate flux of the unmodified membrane decreased to 9.9 LMH. With the same accumulated permeate volume (6 mL) of HAdV-2 suspension, filtered for 100 minutes at the initial permeate flux of 12.1 LMH, the permeate flux

of the modified membrane decreased to 8.6 LMH. Hence, only a minor difference in the flux decline of 33% vs. 29% was detected for the pristine and the modified membrane, respectively.

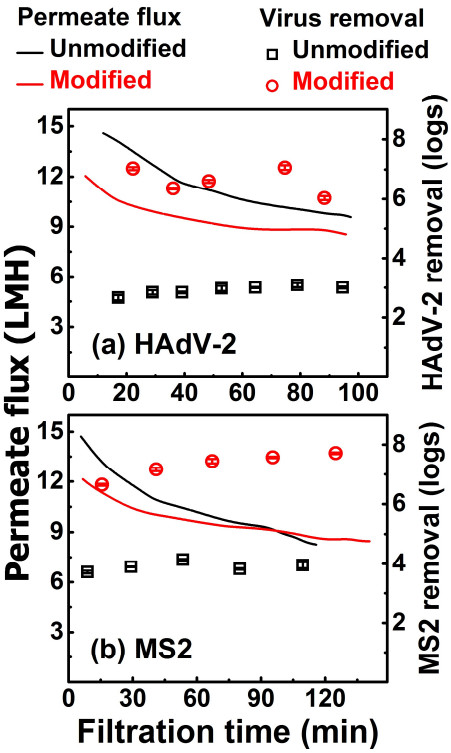

Figure 4.5 The permeate flux (left-Y axis) and virus removal (right-Y axis) were plotted as a function of the filtration time for both the unmodified (black lines and scatters) and the modified (red lines and scatters) membranes.

Similar to HAdV-2, the modified membrane also achieved a higher MS2 removal than the unmodified membrane, as shown in Figure 4.5 (b). The MS2 removal by the modified membrane, 6.6 to 7.8 $\log_{10}$, was much higher than the removal by the unmodified membrane, 3.7 to 4.2 $\log_{10}$. With 10 mL MS2 suspension filtered by both membranes, the permeate flux of the unmodified membrane decreased from 14.6 LMH to 8.2 LMH, while the permeate flux of the modified membrane decreased from 12.2 to 8.5 LMH. The unmodified membrane lost 44% permeate flux during the MS2 filtration, and the modified membrane lost 31%.

MS2 and HAdV-2 filtration by SMP fouled membranes. After fouling the modified and the unmodified membranes with the same amount of SMP (0.13 mg TOC/cm^2), the HAdV-2

removal is shown in Figure 4.6 (a), and the MS2 removal is shown in Figure 4.6 (b). Because of the different quantification methods for the two viruses, it is not valid to compare the MS2 removal and the HAdV-2 removal, since qPCR might detect HAdV-2 genes that penetrated the membranes, and the PFU assay would only detect infectious MS2. For the modified membrane with SMP foulants, the HAdV-2 removal was between 5.3 and 6.4 $\log_{10}$. The unmodified membrane achieved HAdV-2 removals between 3.9 and 5.0 $\log_{10}$ in the presence of SMP foulants. For MS2 removal by SMP fouled membranes, the modified membrane achieved 8.4 to 9.0 $\log_{10}$, compared to the 2.9 to 3.6 $\log_{10}$ observed for the unmodified membrane. The modified membrane achieved higher virus removal after SMP fouling, for both MS2 and HAdV-2.

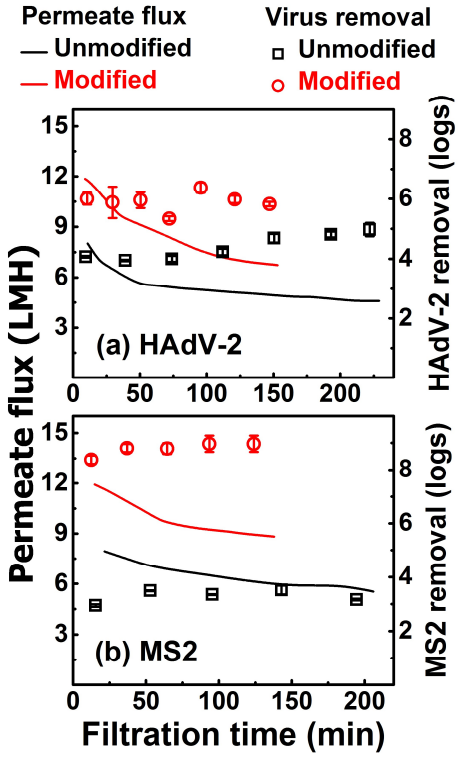

Figure 4.6 The permeate flux (left-Y axis) and virus removal (right-Y axis) were plotted as a function of the filtration time for both the unmodified (black lines and scatters) and the modified (red lines and scatters) membranes after SMP fouling.

In virus filtration after SMP fouling, the permeate flux of the modified membrane was higher than that of the unmodified membrane, as shown in Figure 4.6 (a) and (b), at the same applied pressure of 0.69 bar. The higher permeate flux of the modified membrane is due to the reversible SMP fouling as shown in Figure 4.7. The permeate flux of the modified membrane decreased

from 12.3 to 7.6 LMH (38%) with SMP foulants of 0.13 mg TOC/cm^2, and the unmodified membrane was from 14.8 to 9.1 LMH (39%). When the influent was changed from SMP to MS2, the permeate flux of the modified membrane recovered to 11.9 LMH. The unmodified membrane did not recover the permeate flux by changing the influent solution. Similar permeate flux recovery was also observed in measuring the permeate flux with DI water after the MS2 filtration for the modified membrane, but not for the unmodified membrane (Figure 4.7 (a) and (b)).

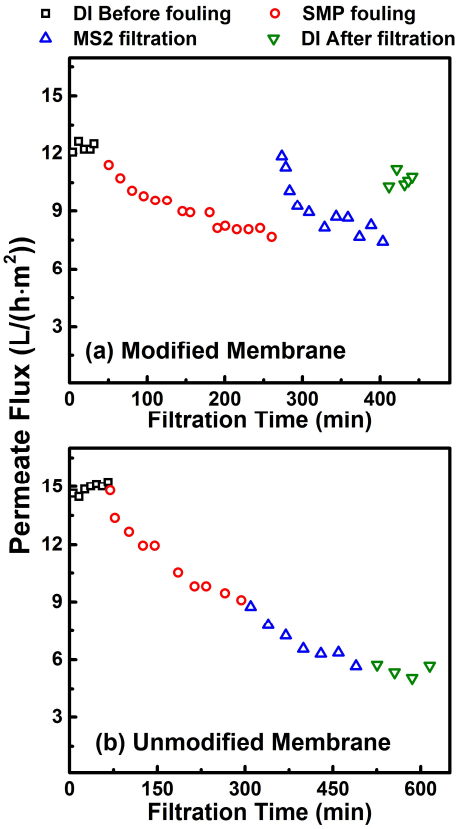

Figure 4.7 The permeate flux for the clean membrane measured with deionized water (DI) (black square), during SMP fouling (red circles), during MS2 filtration (blue triangle), and after MS2 filtration with DI (green inverse triangle) for the modified (a) and the unmodified (b) membranes.

4.5 Discussion

Even though the size of MS2 and HAdV-2 are larger than the nominal molecular weight cut-off of the unmodified membrane (150 kDa) [36, 37], viruses were still detected in the effluent for both the modified and the unmodified membranes. This observation is consistent with a previous characterization of similar membranes that dextran of 400 kDa could penetrate the membrane [38]. We suggest that the virus probably penetrate the membrane through the abnormal large pores and the membrane imperfection. which has been previously reported for bacteria spores [39].

Though membrane imperfection presented on both the modified and the unmodified membranes, significantly higher virus removals were observed for the modified membrane, as shown in Figure 4.5. We attribute the lower virus removal by the unmodified membrane to the accumulation of the rejected viruses near the membrane surface, which increased the local virus concentration [21]. Based on a previous analysis of the velocity field of ultrafiltration membranes [40], viruses near the abnormal large pores would probably be dragged towards the large pores due to the high water flow velocity towards the pores. For the modified membrane, the polySPP layer acted as a barrier that prevented viral particles from approaching the membrane surface. The AFM data presented in Figure 4.3 shows a longer repulsive range on the modified membrane compared to the unmodified membrane, which is consistent with previous studies on polySPP hydration [41, 42]. The long repulsion force exerted by the polySPP layer resulted in virus rejection at a longer distance away from the membrane surface. The previous flow velocity analysis [40] reported that the convection transport of viruses towards membrane pores is weaker when the distance between rejected viruses and the membrane pores is larger. As a result, virus accumulation on the membrane surface is more likely to occur on the unmodified membrane, leading to a higher local virus concentration, and therefore a lower virus removal was observed.

The observed virus removal enhancement by membrane modification, shown in Figure 4.5, could be reasonably attributed to the polySPP layer attenuating virus accumulation on the membrane surface, based on the analysis below. As previously reported [15], the virus concentration in the permeate is determined by the intrinsic removal of the membrane and the local virus concentration at the membrane surface, $C_{membrane}$, as shown in equation (3).

$$\text{Intrinsic virus removal } (log_{10}) = -log_{10}\frac{C_{permeate}}{C_{membrane}} \quad (3)$$

$C_{membrane}$ is estimated for two cases: 1) assuming the occurrence of virus accumulation on the membrane surface and 2) assuming no occurrence of virus accumulation on the membrane surface. With viruses accumulating on the membrane surface, $C_{membrane}$ cannot be higher than the concentration of MS2 in a hexagonal packing, which is 3.94×10^{16} MS2/mL, with the MS2 diameter being 33 nm in the calculation. In the case assuming no virus accumulation, $C_{membrane}$ is the same as $C_{influent} = 2.3\times10^{9}$ MS2/mL. Comparing the two assumed cases, the difference of MS2 removal would be 7 $\log_{10}$, while the observed MS2 removal difference between the modified and the unmodified membranes was 3-4 $\log_{10}$. Similarly, a 5 $\log_{10}$ difference of HAdV-2 removal is calculated for the assumed cases, while the observed difference between the unmodified and the modified membranes was around 3 $\log_{10}$. The observed virus removal differences between the modified and the unmodified membranes are smaller than the theoretical predictions because: 1) the actual $C_{membrane}$ on the unmodified membrane is lower than the hexagonal packing concentration [43]; 2) the $C_{membrane}$ on the modified membrane surface would be higher than $C_{influent}$, despite the fact that the polySPP layer weakens the virus accumulation. In summary, the virus removal enhancement by the membrane modification observed in our experiment does not exceed the theoretical limit, considering that virus accumulation was attenuated by the polySPP layer.

Besides being a barrier inhibiting viruses approaching the membrane surface, the zwitterionic characteristic of the polySPP layer likely reduces virus adsorption, as evidenced with the permeate flux shown in Figure 4.7. The permeate flux decline caused by SMP and MS2 adsorption onto the modified membrane was reversible, while it was irreversible on the unmodified membrane. The neutral complexes of the polyelectrolyte groups bearing opposite charges is likely to cause a low affinity of viruses to the polySPP layer [44, 45]. In addition, the polySPP coating also influences the virus transport within the membrane pores. The ATR-FTIR (Figure 4.2) and the contact angle (Table 4.1) data validate that the polySPP coating changes the membrane structure even on the outlet side of the membrane. The polySPP coating within the membrane pores could influence the virus removal due to the interaction forces between viruses and the polySPP layer. Recently, the significance of virus-membrane interaction force on virus retention within the membrane pores has been recognized [18], and the virus retention within the membrane pores has been proven to influence the observed virus removal [23]. As shown in

Figure 4.7, the reversible permeate flux of the modified membrane indicates less virus and SMP adsorption onto the polySPP layer in the pore channels compared to the unmodified membrane. Future study is needed to understand in detail how the change of virus transport within the membrane pores caused by membrane modification could result in the enhanced virus removal by the modified membrane.

For virus filtration by the SMP fouled membranes, the foulants did not significantly change the virus removal and the permeate flux of the modified membrane. The likely reason for this observation is that the low adsorption of foulant on the modified membrane did not change the membrane structure and the virus-membrane interaction force. The HAdV-2 removal of the unmodified membrane was greatly increased by SMP foulants, accompanied by a significant decrease of the permeate flux, as shown in Figure 4.5 (a) and Figure 4.6 (a). Similar observation has been reported and discussed in previous studies [12, 13, 16]. For MS2 filtration with the SMP fouled unmodified membrane, the permeate flux decreased significantly compared to the clean membrane, but the MS2 removal showed no difference. Our interpretation is that the SMP foulants caused a decrease in the pore size of the abnormal large pore size, leading to the observed increase of the HAdV-2 removal. The size of MS2 was much smaller than HAdV-2, and thus the pore size decrease has no influence on MS2 going through the abnormal large pores.

4.6 Conclusion

- The polySPP hydrogel layer grafted onto the membrane surface exerted repulsion forces towards particles approaching the membrane.
- The range of the repulsive forces on the polySPP grafted membrane was longer than that for the unmodified membrane and thus the virus removal efficiency got enhanced due to the weakened virus accumulation on the modified membrane surface.
- The graft-polymerization increased the virus removal to higher than 6.0 $\log_{10}$ for both the small size MS2 and the large size HAdV-2.
- Fouling with the SMP did not significantly change the virus removal and the permeate flux of the polySPP modified membrane.

Acknowledgements. We want to thank Xia Shang and Darold Marrow for their help with the filtration unit design, and Professor Saikaly and Dr. Matar at KAUST for the LC-OCD data. This project was partially supported by grant RD83582201-0 from the U.S. Environmental Protection Agency (EPA). Its contents are solely the responsibility of the grantee and do not necessarily represent the official views of the EPA. Further, the EPA does not endorse the purchase of any commercial products or services mentioned in the publication. This work was also partially supported by the German-Israeli Water Technology Cooperation Program, which is funded by the Ministry of Science & Technology of Israel and the Federal Ministry of Education and Research of Germany (BMBF-MOST, BMBF grant # 02WA1261B, MOST grant # GR-2394).

4.7 References

1. Steinle-Darling, E., J. Sutherland, and A. Salveson, *Sampled Direct Potable Reuse Water Shows Promising Results.* Opflow, 2016. **42**(2): p. 20-22.
2. Wade Miller, G., *Integrated concepts in water reuse: managing global water needs.* Desalination, 2006. **187**(1–3): p. 65-75.
3. Simmons, F.J., D.H.W. Kuo, and I. Xagoraraki, *Removal of human enteric viruses by a full-scale membrane bioreactor during municipal wastewater processing.* Water Research, 2011. **45**(9): p. 2739-2750.
4. Campos, C.J.A., et al., *Human norovirus in untreated sewage and effluents from primary, secondary and tertiary treatment processes.* Water Research, 2016. **103**: p. 224-232.
5. USEPA, *Guidelines for Water Reuse, Office of Wastewater Management, Washington, DC. EPA/600/R-12/618.* 2012.
6. Simmons, F.J. and I. Xagoraraki, *Release of infectious human enteric viruses by full-scale wastewater utilities.* Water Research, 2011. **45**(12): p. 3590-3598.
7. Vergara, G.G.R.V., J.B. Rose, and K.Y.H. Gin, *Risk assessment of noroviruses and human adenoviruses in recreational surface waters.* Water Research, 2016. **103**: p. 276-282.
8. Hall, A.J., et al., *The Roles of Clostridium difficile and Norovirus Among Gastroenteritis-Associated Deaths in the United States, 1999–2007.* Clinical Infectious Diseases, 2012. **55**(2): p. 216-223.
9. Fong, T.-T. and E.K. Lipp, *Enteric Viruses of Humans and Animals in Aquatic Environments: Health Risks, Detection, and Potential Water Quality Assessment Tools.* Microbiology and Molecular Biology Reviews, 2005. **69**(2): p. 357-371.
10. Fong, T.-T., et al., *Quantitative Detection of Human Adenoviruses in Wastewater and Combined Sewer Overflows Influencing a Michigan River.* Applied and Environmental Microbiology, 2010. **76**(3): p. 715-723.
11. Ueda, T. and N.J. Horan, *Fate of indigenous bacteriophage in a membrane bioreactor.* Water Research, 2000. **34**(7): p. 2151-2159.
12. Shang, C., H.M. Wong, and G.H. Chen, *Bacteriophage MS-2 removal by submerged membrane bioreactor.* Water Research, 2005. **39**(17): p. 4211-4219.

13. Wu, J., H. Li, and X. Huang, *Indigenous somatic coliphage removal from a real municipal wastewater by a submerged membrane bioreactor.* Water Research, 2010. **44**(6): p. 1853-1862.
14. Huang, H., et al., *Mechanisms of virus removal from secondary wastewater effluent by low pressure membrane filtration.* Journal of Membrane Science, 2012. **409–410**(0): p. 1-8.
15. Mallevialle, J., P.E. Odendaal, and M.R. Wiesner, *Water treatment membrane processes*. 1996: American Water Works Association.
16. Lu, R., D. Mosiman, and T.H. Nguyen, *Mechanisms of MS2 Bacteriophage Removal by Fouled Ultrafiltration Membrane Subjected to Different Cleaning Methods.* Environmental Science & Technology, 2013. **47**(23): p. 13422-13429.
17. Kim, M.-m. and A.L. Zydney, *Effect of electrostatic, hydrodynamic, and Brownian forces on particle trajectories and sieving in normal flow filtration.* Journal of Colloid and Interface Science, 2004. **269**(2): p. 425-431.
18. Dishari, S.K., et al., *Effects of solution conditions on virus retention by the Viresolve® NFP filter.* Biotechnology Progress, 2015. **31**(5): p. 1280-1286.
19. Skibinski, B., P. Müller, and W. Uhl, *Rejection of submicron sized particles from swimming pool water by a monolithic SiC microfiltration membrane: Relevance of steric and electrostatic interactions.* Journal of Membrane Science, 2016. **499**: p. 92-104.
20. Herath, G., K. Yamamoto, and T. Urase, *The effect of suction velocity on concentration polarization in microfiltration membranes under turbulent flow conditions.* Journal of membrane science, 2000. **169**(2): p. 175-183.
21. Lu, R., et al., *Effect of virus influent concentration on its removal by microfiltration: The case of human adenovirus 2.* Journal of Membrane Science, 2016. **497**: p. 120-127.
22. Dishari, S.K., A. Venkiteshwaran, and A.L. Zydney, *Probing effects of pressure release on virus capture during virus filtration using confocal microscopy.* Biotechnology and Bioengineering, 2015. **112**(10): p. 2115-2122.
23. Jackson, N.B., et al., *Internal virus polarization model for virus retention by the Ultipor® VF Grade DV20 membrane.* Biotechnology Progress, 2014. **30**(4): p. 856-863.
24. Eshet, I., et al., *Chemical and Physical Factors in Design of Antibiofouling Polymer Coatings.* Biomacromolecules, 2011. **12**(7): p. 2681-2685.

25. Herzberg, M.H.M., et al., *Surface Properties and Reduced Biofouling of Graft-Copolymers That Possess Oppositely Charged Groups.* Biomacromolecules, 2011. **12**(4): p. 1169-1177.
26. Shannon, M.A., et al., *Science and technology for water purification in the coming decades.* Nature, 2008. **452**(7185): p. 301-310.
27. Bae, J. and K.J. Schwab, *Evaluation of murine norovirus, feline calicivirus, poliovirus, and MS2 as surrogates for human norovirus in a model of viral persistence in surface water and groundwater.* Applied and Environmental Microbiology, 2008. **74**(2): p. 477-484.
28. Belfer, S., Y. Purinson, and O. Kedem, *Surface modification of commercial polyamide reverse osmosis membranes by radical grafting: An ATR-FTIR study.* Acta Polymerica, 1998. **49**(10-11): p. 574-582.
29. Belfer, S., et al., *Surface modification of commercial composite polyamide reverse osmosis membranes.* Journal of Membrane Science, 1998. **139**(2): p. 175-181.
30. Lu, R., Q. Li, and T.H. Nguyen, *Random sequential adsorption of human adenovirus 2 onto polyvinylidene fluoride surface influenced by extracellular polymeric substances.* Journal of Colloid and Interface Science, 2016. **466**: p. 120-127.
31. Huber, S.A., et al., *Characterisation of aquatic humic and non-humic matter with size-exclusion chromatography – organic carbon detection – organic nitrogen detection (LC-OCD-OND).* Water Research, 2011. **45**(2): p. 879-885.
32. Matar, G., et al., *Temporal changes in extracellular polymeric substances on hydrophobic and hydrophilic membrane surfaces in a submerged membrane bioreactor.* Water Research, 2016. **95**: p. 27-38.
33. Butt, H.-J., et al., *Steric Forces Measured with the Atomic Force Microscope at Various Temperatures.* Langmuir, 1999. **15**(7): p. 2559-2565.
34. Gutierrez, L. and T.H. Nguyen, *Interactions between Rotavirus and Suwannee River Organic Matter: Aggregation, Deposition, and Adhesion Force Measurement.* Environmental Science & Technology, 2012. **46**(16): p. 8705-8713.
35. Laspidou, C.S. and B.E. Rittmann, *A unified theory for extracellular polymeric substances, soluble microbial products, and active and inert biomass.* Water Research, 2002. **36**(11): p. 2711-2720.

36. Kuzmanovic, D.A., et al., *Bacteriophage MS2: Molecular Weight and Spatial Distribution of the Protein and RNA Components by Small-Angle Neutron Scattering and Virus Counting.* Structure, 2003. **11**(11): p. 1339-1348.
37. Rux, J.J. and R.M. Burnett, *Adenovirus structure.* Human gene therapy, 2004. **15**(12): p. 1167-1176.
38. Birkner, M. and M. Ulbricht, *Ultrafiltration membranes with markedly different pH- and ion-responsivity by photografted zwitterionic polysulfobetain or polycarbobetain.* Journal of Membrane Science, 2015. **494**: p. 57-67.
39. Mi, B., et al., *Microbial Passage in Low Pressure Membrane Elements with Compromised Integrity.* Environmental Science & Technology, 2005. **39**(11): p. 4270-4279.
40. Pontius, F.W., J.P. Crimaldi, and G.L. Amy, *Virus passage through compromised low-pressure membranes: A particle tracking model.* Journal of Membrane Science, 2011. **379**(1–2): p. 249-259.
41. Yang, Q. and M. Ulbricht, *Novel Membrane Adsorbers with Grafted Zwitterionic Polymers Synthesized by Surface-Initiated ATRP and Their Salt-Modulated Permeability and Protein Binding Properties.* Chemistry of Materials, 2012. **24**(15): p. 2943-2951.
42. Cheng, G., et al., *Zwitterionic carboxybetaine polymer surfaces and their resistance to long-term biofilm formation.* Biomaterials, 2009. **30**(28): p. 5234-5240.
43. Oberholzer, M.R., et al., *2-D and 3-D Interactions in Random Sequential Adsorption of Charged Particles.* Journal of Colloid and Interface Science, 1997. **194**(1): p. 138-153.
44. Ladd, J., et al., *Zwitterionic Polymers Exhibiting High Resistance to Nonspecific Protein Adsorption from Human Serum and Plasma.* Biomacromolecules, 2008. **9**(5): p. 1357-1361.
45. Chen, S. and S. Jiang, *A new avenue to nonfouling materials.* Advanced Materials, 2008. **20**(2): p. 335-+.

CHAPTER 5
CONCLUSIONS

5.1 Conclusion

The dominant factors of virus transport in membrane filtration have been proposed. It is generally accepted that virions in the feed solution transport towards the permeate side of the membrane under convective and diffusive forces. The convective drag force is due to water flow towards the membrane pores, and the diffusive transport is due to that the virus concentration in the permeate side of the membrane is lower than that in the feed side. Beyond this knowledge, details of virus rejection and passing through the membrane are elucidated in this study.

Viruses transporting towards the permeate side of the membrane would be retained by the membrane due to the sieving effect. Since the water flow velocity near the membrane pores is large and the flow direction is towards the membrane pore, virus rejected by the membrane could not diffuse back to the bulk solution, leading to its accumulation in the membrane surface vicinity. The increase of local virus concentration would result in an increase of the virus concentration in the permeate solution. The decrease of virus removal over the filtration time was validated in the bench-scale filtration experiment with nearly no change of the permeate flux.

On the membrane surface and within the pores, the attachment efficiency of virus adsorption depends on the virus-membrane interaction forces. Irreversible virus adsorption was determined in the QCM-D experiment. The kinetics of virus adsorption could be appropriately explained with the random sequential adsorption model. Virions previously adsorbed onto the membrane would exert repulsive forces towards the incoming virions, and thus decrease the rate of virus adsorption. As a result, a full coverage of virus on the membrane requires a relative long time. Virus adsorption onto the membrane would lead to pore blockage and pore restriction, which contributes to the increase of virus removal over time in the filtration experiment. Fitting the permeate flux decrease with the pore blockage and cake filtration model also validates the role of virus adsorption in enhancing the virus removal.

The repulsive virus-membrane force is important in improving virus removal. It is determined that the initial stage of virus removal in membrane filtration is the optimal condition: the virus removal is high without virus accumulation on the membrane surface and the permeate flux of the membrane is also high without virus adsorption onto the membrane. We propose that the key point to increase virus removal without decreasing the water permeate flux is to avoid virus accumulation and adsorption on membrane surface by introducing repulsive virus-membrane interaction forces.

To test the hypothesis, a commercially available ultrafiltration membrane is modified targeting high virus removal. By grafting zwitterionic polymers, repulsive interaction forces are introduced onto the membrane. In bench-scale filtration experiments, the modified membrane achieved a 4 logs higher virus removal than the unmodified membrane for both bacteriophage MS2 and HAdV-2. The high virus removal is due to the zwitterionic polymers inhibiting viruses approaching the membrane surface. For the permeate flux, the modified membrane was 20% lower at the beginning of filtration because the topography of the membrane was slightly changed by the graft polymerization. Though the permeate fluxes of both the unmodified and the modified membrane decreased during virus filtration, the modified membrane recovered its permeate flux after pressure relaxation and the unmodified membrane did not. The reversible decrease of permeate flux suggests that virus adsorption is inhibited by the graft polymers. Similarly, the permeate flux decrease caused by SMP was reversible for the modified membrane and irreversible for the unmodified membrane. After fouling with the same amount of SMP, the modified membrane got both higher virus removal and higher permeate flux than the unmodified membrane. In summary, the graft polymerized membrane is a proof of concept for the mechanism studies.

5.2 Contribution

Mechanisms of virus removal in membrane filtration revealed in this study is a supplement to previous knowledge to reveal the complete process of virus going through the membrane. By simplifying the membrane filtration process, the behavior of virus in the membrane surface vicinity is determined with the dynamic of virus removal. The decrease of virus removal at the

beginning of filtration is an evidence supporting the previously reported concept of virus concentration polarization. The increase of virus removal at the later stage of the filtration reveals the role of virus fouling the membrane on its own removal. This finding is consistent with previous observation of virus removal enhanced by other membrane foulants. The transition of virus removal over filtration time, from the decrease to the increase, suggests that virus concentration polarization is dominant in virus removal only at the initial stage of virus filtration. The causal relationship between the virus behaviors in the membrane surface vicinity and the observed virus removal is determined in this study.

The quantitative study of virus adsorption on membrane determines the importance of virus-membrane interaction forces in virus removal. By tuning the virus-membrane interaction forces, the virus adsorption rate correspondingly decreased with the repulsive forces, because of the change in virus attachment efficiency. Irreversible and monolayer virus adsorption are determined in a wide range of environmental conditions including that of the municipal wastewater, even in the presence of foulants. By knowing the pattern of virus adsorption, it is possible to evaluate the virus adsorption kinetics and capacity on the membrane. More importantly, the degree of virus changing the membrane morphology can be determined.

Since the mechanism study highlights the importance of virus-membrane interaction forces and virus accumulation on the membrane, a trial of improving virus removal is conducted with a zwitterionic graft polymerized membrane. It is different from previously proposed membrane modification methods targeting virus removal. The modified membrane achieves significantly higher virus removal both in the presence and absence of foulants. The enhanced virus removal effect is observed for different viruses covering the size of most viruses in the environment. The repulsion on the membrane surface is proved to be effective avoiding virus accumulation and adsorption. The performance of the modified membrane validates the mechanism study and the modification method shows its promise for future application in the industry.

5.3 Future prospect

Achieving virus removal in water reuse needs to be reliable and cost-effective. Though mechanisms of virus removal in membrane filtration are determined in this study, and a proof of concept shows its promise, there are some uncertainties need to be further studied.

The first issue is the membrane foulants, which is a determinant of the cost of membrane filtration. Though the modified membrane in this study shows its resistance towards SMP foulants, it is not clear yet how the real foulant would affect the permeability of the membrane. Based on the mechanisms proposed in this study and previous work, repulsive forces on the membrane surface is significant in both virus removal and foulant resistance. The difficulty to achieve virus removal and foulant resistance lies in the different surface structure of virus and foulants. The heterogeneity and variety of foulants in water increase the difficulty in membrane production and modification. An optimization of membrane is needed beyond this study.

The reliability of membranes is not considered in this study. Since membrane filtration is operated under pressure, a poor mechanical strength would result in breakage of membranes and therefore the virus leakage into the permeate water. To test the membrane reliability, the filtration needs to be operated in a long term including regular membrane cleaning. The life span of the membrane can be improved by increasing the mechanical strength of the membrane or having a supporting layer. The reliability of the membrane would be significant in both virus control and capital cost.

Other processes can be combined with membrane filtration to remove virus in water use. The widely used MBR in wastewater treatment is a combination of activated sludge and membrane filtration. The role of activated sludge on virus removal is not fully understood yet. If virus adsorbed to the biomass in the activated sludge, the mechanism proposed for mono-dispersed virus in this study cannot be applied. Similarly, coagulation before membrane filtration has also been reported on its potential to increase the virus removal efficiency. Micro-/ultrafiltration followed by reverse osmosis is also an intensively studied process for water reuse. While this study focus on the micro-/ultrafiltration membrane, the virus removal by reverse osmosis membranes and influence on membrane permeability is not clear yet. All these unknown questions imply the future improvement that can be achieved to ensure water safety in water reuse.